Earth-Science Reviews 261 (2025) 105032

Contents lists available at ScienceDirect

Earth-Science Reviews

journal homepage: www.elsevier.com/locate/earscirev

The geomorphology of monoclinal scarps associated with interstratal-dissolution fronts in evaporite formations, illustrated with the Upper Jurassic Arab and Hith formations in Ar Riyadh and Central Saudi Arabia

Francisco Gutiérrez [a,*], Yasser Zabramawi [b], Abdullah Memesh [b], Ahmed M. Youssef [b], Alaa Bahamil [b], Luis Auqué [a]

[a] Department of Earth Sciences, University of Zaragoza, Pedro Cerbuna 12, 50009 Zaragoza, Spain
[b] Saudi Geological Survey, P.O. Box 54141, Jeddah 21514, Saudi Arabia

ARTICLE INFO

Keywords:
Evaporite karst
Dissolution subsidence
Sinkhole
Gravitational deformation
Interior Homocline

ABSTRACT

The downdip migration of dissolution fronts in gently tilted evaporite formations produces updip-facing monoclinal folds and adjacent synformal troughs (depositional basins) in the supra-evaporite strata. These gravitational deformation structures, up to 1000 km long, can be expressed in the landscape as laterally migrating fold escarpments and linear depressions, forming the largest karst features on Earth. Despite their large dimensions and numerous associated practical implications (hydrocarbon, salt, geostorage, water quality, sinkhole hazards), the scientific publications dealing with these interstratal evaporite karst features are rather scarce. This work reviews the available literature on dissolutional edges and associated features developed on dipping salt and gypsum/anhydrite formations. It also analyses the >800 km long dissolution and subsidence belt associated with the updip edge of the Upper Jurassic Arab and Hith anhydrites in the Interior Homocline of central Saudi Arabia, with special focus on its striking geomorphic features. This is the largest Ca-sulphate karst feature in the world, despite the aridity of the region, and is also the example in which the associated landforms and deformation structures are best displayed. It displays striking monoclinal scarps with an aggregate length of 420 km, affected by crestal extensional structures and punctured by numerous giant caprock collapse sinkholes. The increased sinkhole hazard and risk documented in the Ar Riyadh area in recent times can be attributed to adverse human activities (localized artificial water input) and the expansion of the urban area across the dissolution front and monoclinal scarp.

1. Introduction

In the first part of this work we review the existing worldwide literature on dissolution and subsidence belts associated with the updip edge of evaporites, including salt and gypsum/anhydrite formations. In the second part we focus on the subsidence belt associated with the Arab and Hith anhydrites in the Interior Homocline of central Saudi Arabia, paying especial attention to its striking landforms (e.g., monoclinal fold escarpments, giant caprock collapse sinkholes), as well as the associated ground instability hazards. A number of remarkable features concur on this case study: (1) it is the longest Ca-sulphate karst feature in the world, with more than 800 km in length, despite the aridity of the environment; (2) it is the evaporite dissolution and subsidence belt where the associated geomorphic features and deformation structures are best displayed; (3) the Arab and Hith anhydrites are the seal of some of the world's most prolific petroleum systems (Murris, 1980; Ayres et al., 1982; Alsharhan and Kendall, 1986; Al-Mojel et al., 2020), including the Ghawar field, which is the world's largest reservoir (Lindsay et al., 2006); (4) the capital of Saudi Arabia, Ar Riyadh, with around 8 million inhabitants, largely lies on the dissolution and subsidence trough, and is facing increasing environmental problems (e.g., sinkholes, pollution) as it expands towards the dissolution front (e.g., Cueto et al., 2018; Al-Hashim et al., 2024); (5) the Hith Anhydrite Formation has been considered as a candidate for a CCUS project (CO2

* Corresponding author.
E-mail address: fgutier@unizar.es (F. Gutiérrez).

https://doi.org/10.1016/j.earscirev.2024.105032
Received 5 September 2024; Received in revised form 12 December 2024; Accepted 18 December 2024
Available online 26 December 2024

capture, utilization and storage), which could maintain pressure in the intra-formation and underlying reservoirs (Wolpert et al., 2024).

2. Literature review

Dissolution acting on an evaporite formation overlain by non-soluble or less soluble rocks (caprock) is commonly referred to as interstratal karst. Evaporite rocks, and especially salt, because of their frequent lack of internal permeability, often dissolve through the migration of dissolution fronts. The edges in contact with undersaturated groundwater flows recede inwards, and the evaporitic body shrinks like a melting block of ice. The partial or complete dissolution of an evaporite formation leaves behind (Warren, 2016; De Waele and Gutiérrez, 2022): (1) dissolution residues consisting of the insoluble (e.g., clay, marls) or less soluble (e.g., limestone, anhydrite) components of the formation; and (2) solution-collapse breccias produced by the fragmentation and settling of overlying and interbedded strata. Interstratal dissolution by migrating dissolution fronts entails a reduction in the thickness of the stratigraphic succession and the subsidence of the overlying rocks and the ground surface. Given sufficient time and adequate geological conditions, evaporite formations, and especially salts, eventually vanish by dissolution. According to Warren (2016), there are probably more intervals of dissolution residues in the stratigraphic record than remaining salt beds.

Dissolution fronts are commonly associated with the shallow edge of evaporite formations (e.g., updip edge of dipping units, diapir crest) that is flushed away by meteoric waters in the telogenetic zone (epigene dissolution). Interstratal karst may be also related to deep-seated meteoric or basinal flow systems that can cause hypogene dissolution from below, often controlled by permeability features in the substrata such as fractures or reefs. Interstratal evaporite dissolution is frequently an unappreciated process due to its hidden character, large spatial-temporal scale, and relatively slow rates. Its investigation requires multidisciplinary studies addressing the multiple evidence produced and induced by dissolution and gravitational deformation phenomena (e.g., Kirkham et al., 2002; Gutiérrez et al., 2014; Johnson, 2021a; De Waele and Gutiérrez, 2022 and references therein): (1) The main stratigraphic evidence includes the insoluble residues and solution-collapse breccias, postdepositional thickness changes exhibited by the partially dissolved evaporite units, the sediments accumulated in dissolution-induced basins, and chemical deposits and other precipitates (e.g., cements, nodules) related to the recycling of the dissolved evaporites. The age and geometrical features (e.g., thickness changes, growth strata) of the sediments filling subsidence basins can provide information on the timing of the dissolution and subsidence episodes. (2) Structural evidence is provided by a wide variety of ductile and brittle deformation structures developed in the overlying units as a result of subsurface mass depletion. These are gravitational structures restricted to the units situated above the dissolution zone. (3) The geomorphic evidence corresponds to the multiple landforms produced by the subsidence process (e.g., sagging basins and troughs, fold and fault scarps, grabens, sinkholes), and the effects of the latter on geomorphic systems (e.g., disrupted drainages, creation of lake basins). (4) Hydrochemical evidence of interstratal dissolution is offered by the high-salinity waters that have interacted with the evaporites and emerge at springs and groundwater output zones. The flow rate and solute concentration could be used to estimate rates of subsurface dissolution, although no examples have been found in the scientific literature.

In gently dipping successions, the interstratal dissolution of evaporites commonly occurs by the down-dip migration of dissolution fronts. Gravitational bending of the overlying strata produces a strike-parallel monoclinal fold atop the dissolution front and an adjoining asymmetric synform (subsidence trough) (Gutiérrez and Cooper, 2013; Warren, 2016; De Waele and Gutiérrez, 2022). The monoclinal folds can be expressed in the landscape as long and prominent fold scarps punctured by sinkholes and affected by secondary bending-moment faults (extensional structures, buckle folds). The subsidence troughs may function as laterally migrating depositional basins and tend to control the hydrographic network (e.g., rivers, lakes). These dissolution and subsidence belts are the largest karst features on Earth (De Waele and Gutiérrez, 2022). The subsidence belt related to the dissolution of the gently dipping Middle Devonian Prairie Evaporite in western Canada reaching around 1000 km long in Canada as detailed below (Broughton, 2017, 2021). Moreover, these dissolution and subsidence features have numerous practical implications for the development of resources (e.g., salt, hydrocarbon), geostorage operations (e.g., nuclear waste, hydrocarbons), water management (e.g., hydrochemical degradation of underground and surface water), and geohazard assessment, particularly subsidence and sinkholes. Despite their large size and importance for the applied perspective, the available information in scientific publications on these evaporite karst features is rather limited.

Dissolution fronts associated with the updip edge of gently dipping evaporites, mainly salt but also in gypsum/anhydrite, occur in a number of regions worldwide. These interstratal dissolution features are accompanied by updip-facing monoclines and adjoining subsidence troughs. Both gravitational deformation structures, restricted to the supra-evaporite strata, may be expressed in the landscape as fold scarps and topographic lows at their foot, respectively. Apart from the case of the Upper Jurassic anhydrites in Saudi Arabia, the documented down-dip migrating dissolution fronts essentially occur in: (1) large evaporite basins of Paleozoic age (i.e., Permian, Devonian); (2) basins that have experienced limited tectonic deformation, such as gentle tilting; and (3) areas subject to intense geological investigations, largely related to oil exploration and production (e.g., North America, Arabian Peninsula).

In western Canada, the SW-dipping Middle Devonian Prairie Evaporite of the Elk Point Group, up to 200 m thick and dominated by halite, has been affected by multiple phases of interstratal dissolution along its northeastern up-dip edge (average annual precipitation in Saskatoon, ~350 mm/yr). The propagation of the dissolution front has resulted in subsidence in the overlying Middle-Upper Devonian carbonate strata and other formations overlying a sub-Cretaceous unconformity (De Mille et al., 1964; Anderson and Knapp, 1993; Walker et al., 2017). The long-term interstratal dissolution has generated a NW-SE oriented dissolution and subsidence belt around 1000 km long and as much as 150 km wide, considered as the largest karst feature worldwide (Broughton, 2017, 2018a, 2021) (Fig. 1). This mega dissolution-induced subsidence belt comprises a broad zone of complete salt removal to the NE, and a zone around 20 km wide of partial salt dissolution underlain by a NE-facing dissolution front at around 200 m depth, locally known as the “salt scarp”. Note that this is not a topographic feature, but a transtratal dissolution boundary in the subsurface. The deep-seated dissolution of the evaporites is related to rising groundwater flow from the underlying carbonate aquifer (Keg River Formation), which has its main recharge area at its NE updip erosional edge (Walker et al., 2017). The initiation of the main salt dissolution phase occurred associated with the Cordilleran-Laramide tectonism (Middle Jurassic - Early Cretaceous), when uplift, tilting and surface erosion created favourable hydrogeological conditions for interstratal karst development (Stoakes et al., 2014; Broughton, 2018a, 2018b) (Fig. 1). Interstratal salt dissolution and subsidence has locally controlled the deposition and architecture of the Early Cretaceous oil sands of the McMurray Formation (main unit of the Athabasca Oil Sands), which is one of the largest sources of unconventional oil (bitumen) in the world. This formation with growth stratal geometries locally fills dissolution basins with more than 100 m of structural relief, recording synsedimentary dissolution-induced subsidence and displaying striking breccia pipes, as well as sagging and collapse paleosinkholes (Hopkins, 1987; Broughton, 2013, 2015, 2017; Walker et al., 2017). The relief of the highly irregular sub-Cretaceous unconformity at the base of the McMurray Formation is largely related to differential dissolution-induced subsidence (Walker et al., 2017). An additional important phase of salt dissolution occurred

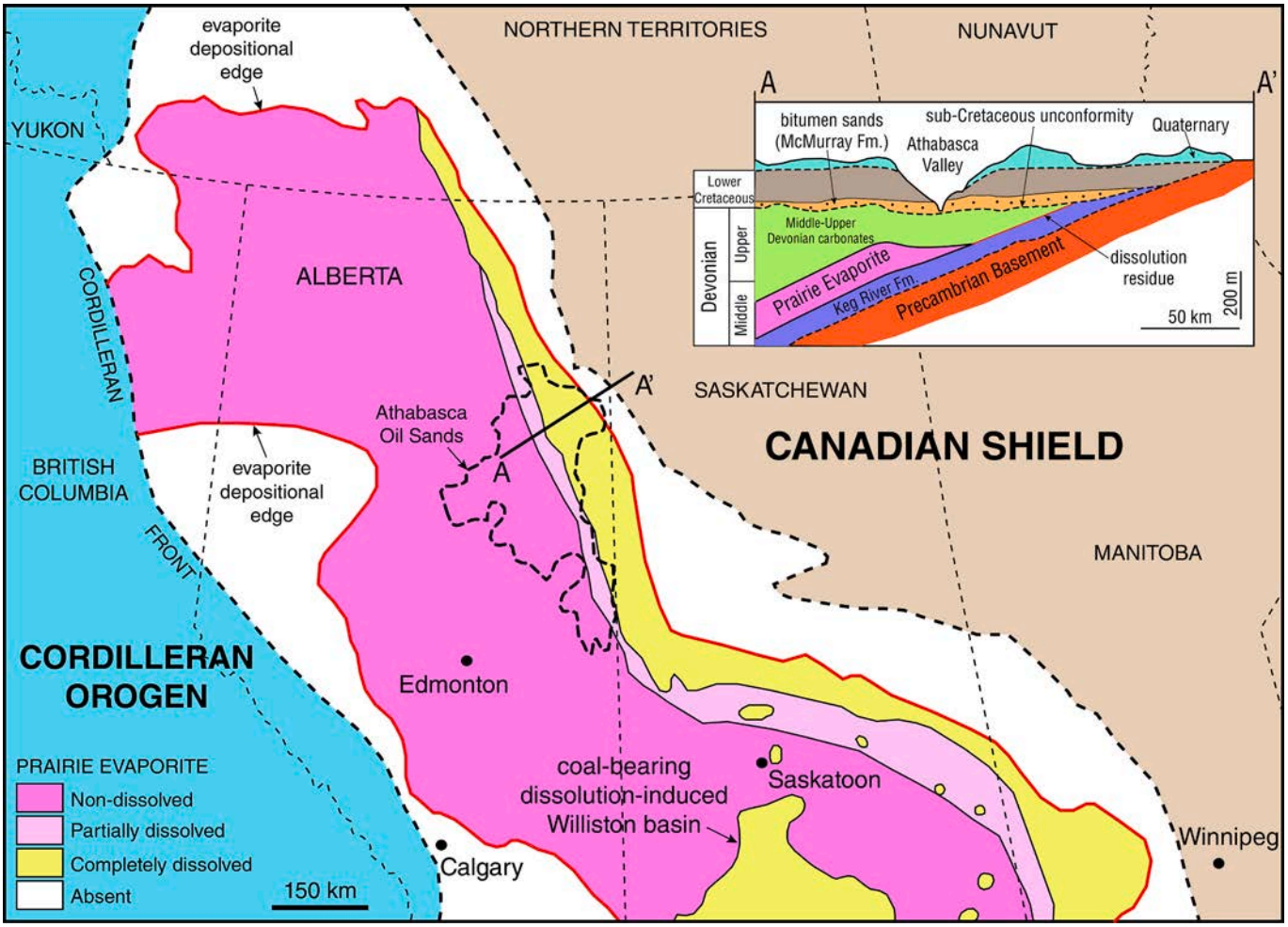

Fig. 1. Map showing the distribution of the dissolution and subsidence belt associated with the updip edge of the Middle Devonian Prairie Evaporite in western Canada, and simplified cross section showing the relationships between the dissolution front, the Lower Cretaceous Athabasca Oils Sands (McMurray Formation) and the Athabasca River valley. Adapted from Broughton (1977, 2013, 2018a).

during the Pleistocene glaciations in relation with glacial loading and enhanced recharge of meltwater (Anderson and Hinds, 1997). The SW migrating topographic low associated with the subsidence belt has controlled morpho-sedimentary environments at least since the Cretaceous. In Early Cretaceous times it functioned as a paleovalley followed by the north-flowing continental-scale McMurray longitudinal drainage system (Broughton, 2018a). During the Pleistocene, glacial ice deepened and expanded the subsidence low and in post-glacial times subsidence troughs over the dissolution front controlled the distribution of lakes and the drainage network, including the North Saskatchewan River (Anderson and Hinds, 1997) and the Athabasca River (Broughton, 2013, 2018a), as proved by seismic profiles and borehole data. It seems that in this case, where the 1.5–2 km thick Laurentide ice sheet caused major erosion, the current geomorphic imprint of the dissolution-induced subsidence phenomenon is the creation of subtle topographic lows that guide the drainage network and host lakes, but the edge of the dissolution front is not expressed by a monoclinal scarp. Saline springs along the Athabasca River valley (Alberta), with TDS values as high as 100 g L^{-1}, provide hydrochemical evidence for the active salt dissolution by meteoric waters that is currently affecting the Prairie salt, as revealed by the chemical characteristics and isotopic signatures of the brines (Birks et al., 2018).

In the Holbrook Basin, Arizona, the up to 300 m thick Permian Supai Salt (renamed as the Corduroy Member of the Schnebly Hill Formation; Blakey, 1990), dipping 2° to the NE, is affected by a NE-propagating dissolution front overlain by a sinuous monoclinal fold scarp around 100 km long known as the Holbrook Anticline (average annual precipitation in Holbrook, ~210 mm/yr). (Fig. 2). Salt dissolution at around 200 m depth has gravitationally folded the overlying Permian and Triassic formations, generating a SW-facing monocline with geomorphic expression (i.e., Pink Cliffs). The strata in the middle limb of the monocline show abrupt dip reversal, dipping as much as 40°SW, whereas the formations underlying the salt are not affected by this supra-salt gravitational structure, which structural and topographic reliefs of approximately 100 m and 60 m, respectively. The crest of the monoclinal scarp displays abundant longitudinal extensional structures hundreds of meters long related to outer-arc stretching, including fissures, scarps and grabens. Pressure ridges up to 8 m high related to inner contraction and buckling folding are common at the lower hinge of the monocline. The scarp is punctured by more than 500 caprock collapse sinkholes up to 200 m across, which show a markedly clustered distribution. The main cluster, known as The Sinks, includes around 250 sinkholes (Fig. 2). Large depressions and playa lakes occur in the piedmont next to the scarp, such as Dry Lake Valley, covering 325 km^2. These enclosed depressions are related to the combination of differential sagging subsidence, sinkhole coalescence, and the development of nested and intersecting sinkholes. At least four major sudden drainage events via sinkholes and fissures, collectively involving a loss of 12.7 million m^3, have been reported in these depressions (water table at 100–150 m depth). Interstratal salt dissolution is caused by groundwater from the overlying Coconino aquifer (top-to-bottom epigene dissolution), with recharge areas in the dipslope to the SW and in the

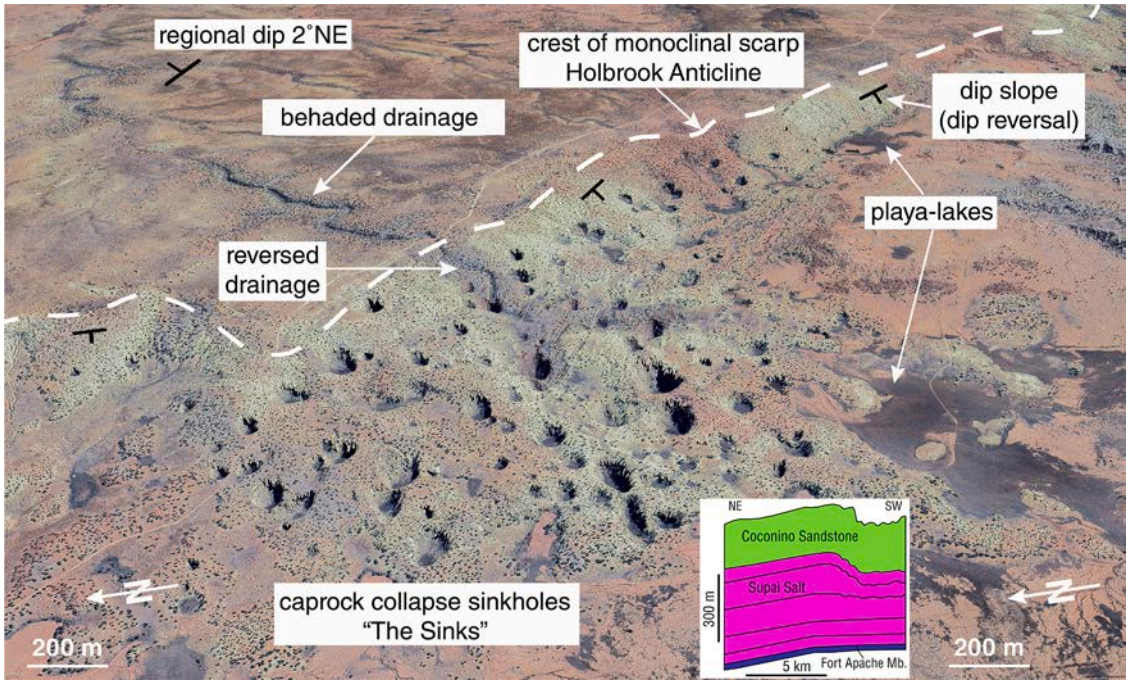

Fig. 2. Oblique view of the Holbrook dissolution-induced monoclinal scarp in Arizona and associated geomorphic features. Note transverse drainage disrupted by counter-dip bending above the dissolution front. Image captured from Google Earth. Inset shows cross-section across the The Sinks showing interstratal dissolution in the upper part of the Supai Salt and subsidence in the overlying Coconino Sandstone (adapted from Neal et al., 2013).

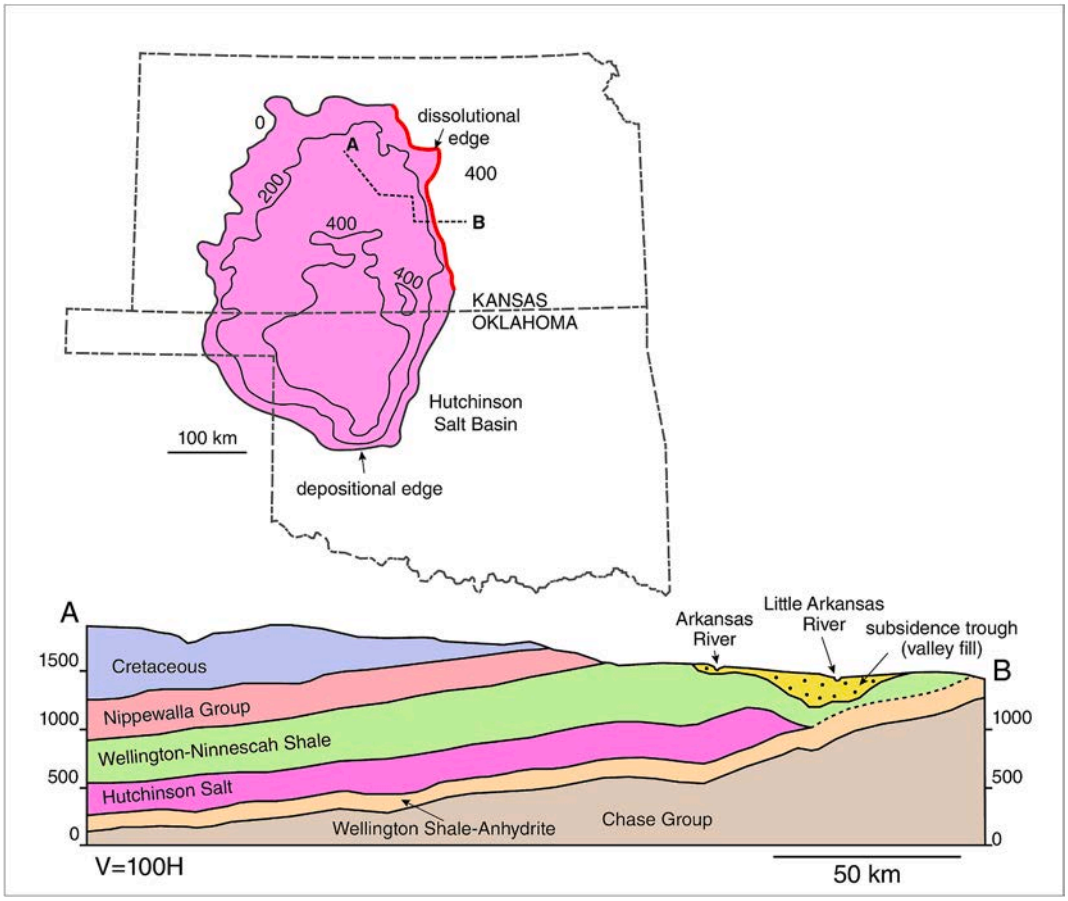

Fig. 3. Distribution on the Permian Hutchison Salt in Kansas and Oklahoma, the updip eastern limit of which corresponds to a westward-migrating dissolutional edge. Contours indicate thickness in feet. Cross section based on borehole data showing the spatial association between the dissolution front of the Hutchinson Salt and a subsidence trough filled with thickened late Tertiary-Quaternary deposits, as well as the Arkansas and Little Arkansas rivers. Adapted from Walters (1978).

subsidence belt, where fissures and sinkholes function as effective infiltration paths. The Coconino aquifer shows elevated values of TDS and high sodium and chloride contents associated with the Holbrook Anticline. The onset of the dissolution and subsidence phenomena is ascribed to the activation of the current groundwater flow system by the uplift and tilting of the Colorado Plateau at least since Pliocene times (Neal, 1995, 1998; Neal and Colpitts, 1997; Neal and Johnson, 2003; Neal et al., 2013). DInSAR studies reveal ongoing subsidence at rates of ca. 4 cm/yr in large topographic basins with nested sinkholes NE of the Holbrook monoclinal scarp (Conway and Cook, 2013).

In NE England, coastal Yorkshire and Teeside, dissolution fronts occur on east-dipping gypsum-anhydrite and halite units of Permian age deposited on the western margin of the Zechstein Basin. These up-dip dissolution boundaries are overlain by west-facing subsidence monoclines on overlying mudstone-rich strata (average annual precipitation in Darlington, ~750 mm/yr). The anhydrite-gypsum transition in the lower evaporite unit occurs at 60–120 m depth. The depth of the dissolution front ranges from 20 to 120 m and the monocline is expressed as a fold scarp with a local relief of 20–40 m equivalent to the thickness of the gypsum-anhydrite unit. The path of post ice-age fluvial systems such as the Skerne River in Darlington and the Ure River at Ripon was guided by the monoclinal scarp and the associated subsidence trough. The dissolution front developed on the more soluble 50 m thick halite unit lies at a significantly greater depth range of 300–400 m, and the overlying monocline, inferred from boreholes, does not display any topographic expression. It has been suggested that the deep-seated dissolution in the salt bed has been favoured by elevated hydraulic heads reached during the last glaciation (Late Pleistocene, Devensian),

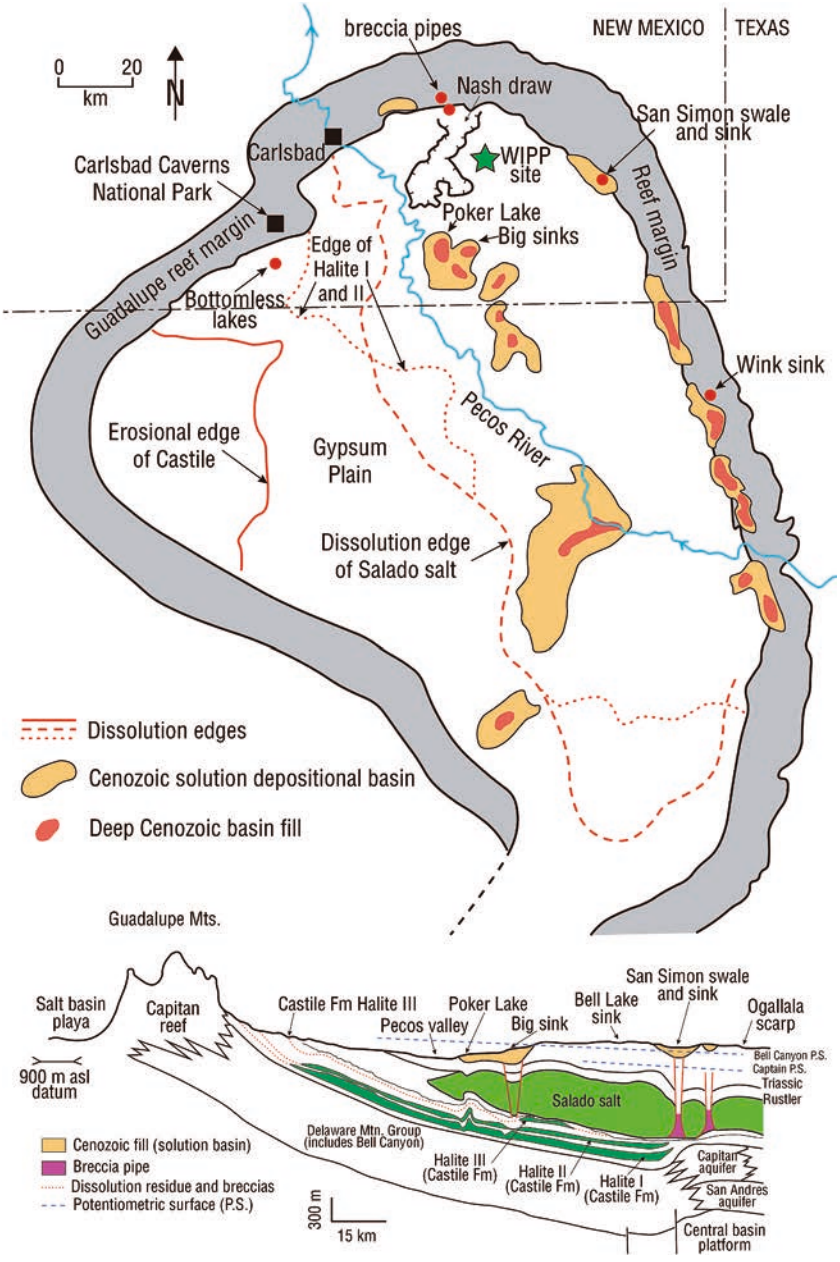

Fig. 4. Simplified map and generalized cross-section of the east-tilted Delaware Basin in Texas and New Mexico. The sketches show the location of the east-migrating dissolution fronts in the Permian Castile and Salado salt formations, and the distribution of two belts of dissolution-induced depositional basins, mainly located east of the Capitan reef and along the Pecos River valley. This fluvial system functions as the regional base level and its position has experienced significant shifts in the Cenozoic. Nash Draw is a dissolution-induced depression with nested collapse structures situated in the vicinity of WIPP site (low-level radioactive waste repository). Adapted from Anderson (1981), Hill (2003) and Warren (2016).

when northern England was buried by a thick and wet-based ice sheet (Cooper, 1998, 2002, 2020).

In central Kansas, a 150 km long dissolution front occurs along the updip edge of the W-dipping and 90 m thick Permian Hutchinson Salt, extending from Salina to Wichita (average annual precipitation in Salina, ~810 mm/yr). (Fig. 3). The salt edge, at 100–150 m depth, has receded around 25 km since the late Tertiary, generating a subsidence belt with sinkholes (Frye, 1950) underlain by valley fill deposits dominated by fluvial and eolian facies. Seismic and borehole data show a clear correlation between leached Permian salt and thickened Quaternary deposits, the chronology of which can be locally constrained by the Pearlette Ashes that originated from the Yellowstone caldera in Wyoming (0.62–2.02 Myr) (Fig. 3). Remnants of salt are locally identified east of the dissolution front, revealing incomplete salt dissolution in some sectors. Although the dissolution front lacks any clear geomorphic expression (e.g., monoclinal scarp), the subsidence belt controls the path of major drainages such as the Arkansas and the Little Arkansas rivers (Fig. 3). In this case, dissolution advances top-to-bottom (epigene karstification) and it is considered that subsidence contributes to self-sustain the process by increasing the permeability of the strata atop the dissolution front. Active salt dissolution leads to the hydrochemical degradation of both underground and surface waters in central Kansas (Anderson et al., 1994). Walters (1978) indicate an average rate of 3–6 km Myr^{-1} for the horizontal retreat of the dissolution front during the Quaternary. This author also provides a review on human-induced subsidence problems associated with salt mining and oil and gas operations, mostly distributed close to the dissolution front where the salt is situated at shallow depth.

The Delaware Basin, west Texas and southeast New Mexico, is an eastward tilted Permian basin, with the Capitan Reef limestone (Guadalupe Mountains) exposed on the western margin (average annual precipitation in Carlsbad, ~300 mm/yr). (Fig. 4). Here, the evaporite formations are affected by down-dip migrating dissolution fronts along their western edge. In the center of the basin, the evaporites are underlain by permeable carbonates and detrital rocks, including the Capitan Reef limestone. These infra-salt formations include prolific hydrocarbon reservoirs and are the source of upward flows responsible for the hypogene dissolution of the evaporites. Interstratal dissolution of the Late Permian Castile, Salado and Rustler formations have generated dissolution-induced depositional basins (subsidence troughs) up to 150 km long filled with late Cenozoic terrestrial sediments up to 460 m thick (Olive, 1957; Anderson et al., 1978; Bachman, 1980, 1984; Johnson, 1989; Hill, 1996) (Fig. 4). The dissolution-subsidence troughs in the Delaware Basin are arranged in two NNW-trending belts (Fig. 4). The

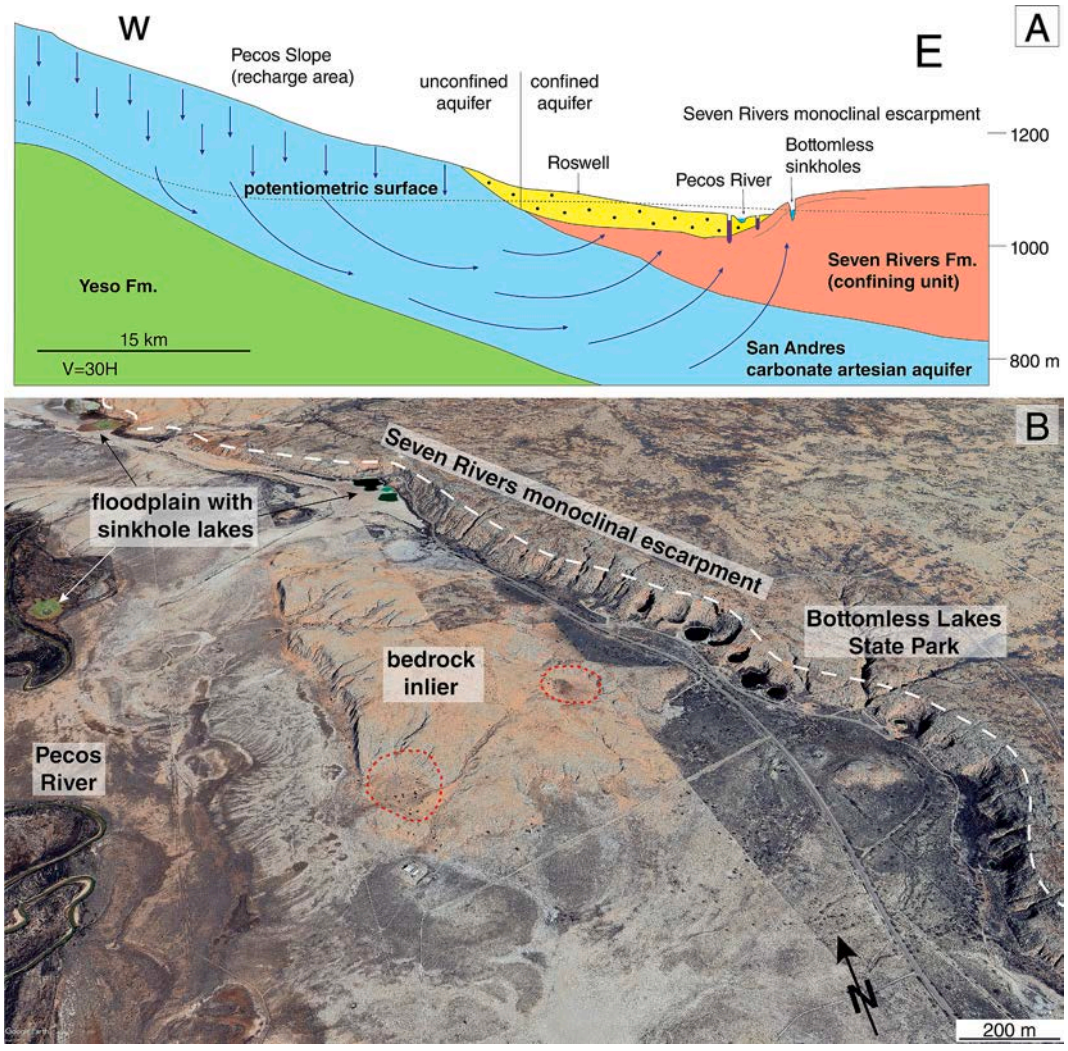

Fig. 5. A: Cross-section of the Roswell Artesian Basin. Groundwater flows downdip in the San Andres carbonate aquifer and discharges upwards into the Pecos River causing hypogene dissolution in the overlying evaporites of the Seven Rivers Formation. The eastern margin of the valley is defined by an E-facing monoclinal escarpment related to differential interstratal dissolution and subsidence (adapted from Land, 2016). B: Oblique image of the Pecos River valley at the Bottomless Lakes State Park. The valley is bounded along its eastern margin by the dissolution-induced Seven Rivers monoclinal scarp. The scarp and the floodplain display numerous sinkholes and subsidence depressions that host lakes and wetlands fed by artesian springs.

eastern one occurs atop the buried reef margin (e.g., San Simon Swale, the dissolution trough in the Wink Sink area). The western belt at the basin center is associated with the NNW-directed Pecos River valley (Bachman, 1984), which functions as the regional base level and has experienced significant lateral shifts. According to Anderson (1981), dissolution in this basin with artesian hydrogeological conditions has reduced the original salt units to 30–40 % of their original volume. In a report on the suitability of salt beds for the emplacement of nuclear waste, Bachman and Johnson (1973) inferred an eastward retreat of 37 km for the dissolutional edge of the Salado Formation in southeastern New Mexico. Considering that this lateral migration occurred after deposition of the Ogalalla Formation (i.e., post 4 Myr), they estimated an average lateral propagation rate for the dissolution front of around 9 km Myr^{-1}.

In southeastern New Mexico, north of the Captain Reef of the Delaware Basin, the Roswell Artesian Basin is developed in a Permian succession (backreef shelf sediments) dissected by the N-flowing Pecos River (average annual precipitation in Roswell, ~330 mm/yr). (Fig. 5). The *E*-dipping San Andres carbonate aquifer has its recharge area in outcrops west of the Pecos River valley (The Pecos Slope). The groundwater flows downdip to the east and the aquifer becomes confined where overlain by the Seven Rivers Formation, a leaky aquitard consisting of slightly to moderately permeable rocks, including gypsum, mudstone, dolomite and some halite. The artesian aquifer discharges in the Pecos River through upward cross-formational flows, likely guided by fractures and breccia pipes, causing hypogenic dissolution (bottom-to-top) in the overlying evaporite succession. The eastern margin of the Pecos River is defined by a sinuous E-facing monoclinal scarp (Seven Rivers Escarpment) related to differential interstratal dissolution and subsidence in the Seven Rivers Formation (Fig. 5). This fold scarp is at least 30 km long, has a local relief of 50–80 m and displays a sharp dip reversal in the middle limb, changing in a short distance from 1°E to as much as 40°W. The escarpment is ruptured by extensional morpho-structures along the crestal upper hinge (fissures, scarps, grabens) that favour the development of mass wasting processes. It is also punctured by numerous hectometre-scale collapse sinkholes. Both the scarp and the floodplain of the Pecos River display abundant brackish lakes and wetlands fed by artesian underwater springs associated with breccia pipes, sinkholes and compound subsidence basins (e.g., Bottomless Lakes State Park, Bitter Lake National Wildlife Refuge) (Quinlan et al., 1986; Land, 2003, 2016; Stafford et al., 2008).

The Syracuse Basin (21,000 km^2) in western Kansas and eastern Colorado was traditionally considered as a structural-sedimentary basin outlined by the extent of the Permian age Flowerpot Salt (61–91 m thick) and the younger middle Blaine Salt (14–18 m thick) (average annual precipitation in Syracuse, ~425 mm/yr). However, a thorough investigation largely based on lithological and geophysical logs reveal that the current perimeter of the salt beds corresponds to dissolutional edges. Consequently, the Syracuse Basin is in fact a salt remnant of what were, at one time, much more extensive salt deposits. The inward retreating dissolutional edges are characterised by (Johnson and Timson, 2023): (1) sharp to gentle wedging out of the salt beds grading into dissolution residues and local salt remnants beyond the main dissolution front; (2) gravitational deformation in the supra-salt sediments, including flexed down strata forming monoclines with a structural relief comparable to the thickness of the dissolved salts; (3) no equivalent deformation in the sub-salt sediments; (4) peripheral dissolution-induced subsidence basins filled with late Cenozoic terrestrial deposits (e.g. Ogalalla Formation); (5) topographic lows that guide the drainage network and locally host subsidence depressions (e.g., Great Plains Reservoirs, Kansas) (Johnson, 2021b); (6) recent sinkhole activity (Johnson, 2021c).

In South Dakota, a dissolution front has migrated down-dip and radially away from the Black Hills in the Permian Minnelusa Formation (average annual precipitation in Syracuse, ~455 mm/yr). (Rahn and Davis, 1996; Epstein, 2003). The long-term progression of the dissolutional edge, favoured by the erosional lowering of the base level, has induced the outward displacement of the sites with active subsidence and brine springs. In the Cretaceous Maha Sarakham Formation of Thailand and Laos, consisting of three evaporite intervals sandwiched between red mudstones, the down-dip migration of dissolution fronts has generated a subsidence trough that controls the path of the Nam Theum River (Supajanya and Friederich, 1992; Utha-aroon et al., 1995; Warren, 2016).

3. Geological setting of the interstratal dissolution belt in Central Saudi Arabia

Two main geological domains can be differentiated in the Arabian Peninsula (Steineke et al., 1958a, 1958b), the Arabian Shield and the Arabian Platform (Fig. 6). The Arabian Shield, east of the Red Sea, is a complex of Precambrian igneous and metamorphic rocks locally capped by Cenozoic volcanic rocks, mainly in basalt fields forming the so-called *harrats*. The Arabian Platform to the east corresponds to a thick Phanerozoic succession unconformably overlying the Arabian Shield, which comprises the Interior Homocline and the Interior Platform. The Interior Homocline, where this work is focused, is a belt of Paleozoic to lower Cenozoic rocks bordering the Arabian Shield with a very gentle basinward dip of ca. 1° NE to E and limited tectonic disruption, mostly restricted to broad flexures. This province is characterised by a cuesta landscape with west-facing scarps and broad intervening gently inclined dipslopes (Rausch et al., 2014a, 2014b). In eastern Arabia, the Interior Platform is dominated by nearly flat-lying outcrops of Cenozoic sedimentary rocks (Alsharhan and Kendall, 1986; Pollastro et al., 1988; Lindsay et al., 2006).

The strike in the gently dipping Phanerozoic formations of the Interior Homocline change abruptly from NW-SE to NN*E*-SSW at Al Kharj (south of Ar Riyadh), defining the Central Arabian Arch (Powers et al., 1966) (Fig. 6). This upwarp, together with the eastward tilting of the arcuate Phanerozoic belt has been ascribed to the late Cenozoic rifting of the Red Sea (Vaslet et al., 1991). At the hinge zone of the Arabian Arch, the Interior Homocline is disrupted by a system of E-W-trending grabens, known as the Central Arabian Graben System (Karpoff, 1956; Hancock and Al-Kadhi, 1978; Breton et al., 1984; Vaslet et al., 1991). This extensional system comprises an array of narrow grabens west of Al Kharj (Buayja, Rufa, Awsat-Ujman and Nisah grabens), and a single and wider graben (Mugharah Graben) east of that locality (Fig. 7). The graben system controls a contributory E-flowing drainage network converging at the Al Kharj water gap (i.e, valley that traverses perpendicularly a ridge or escarpment) and Wadi as Sabha that flows along the Mugharah Graben. Weijermars (1998) and Bamousa et al. (2020) analyse the disruption and re-arrangement of the drainage network associated with the development of these neotectonic grabens, allegedly with a left-lateral displacement component. Geological mapping reveals that late Neogene and probably Quaternary sediments are offset by the graben-bounding faults (Vaslet et al., 1991).

The stratigraphic succession relevant to this work includes Mesozoic formations deposited on the proximal sector of the Arabian Platform, where sedimentation was mainly controlled by climate-related eustatic changes and limited tectonic disruption. From the paleogeographic perspective, the platform was located on the eastern margin of Gondwana, facing the Neo-Tethys Ocean to the east (Lindsay et al., 2006; Al-Mojel et al., 2020). The Upper Jurassic evaporite-bearing Arab and Hith (or Heet) formations are underlain by a conformable Middle-Upper Jurassic carbonate succession including in ascending order the Tuwayq Mountain Limestone, the Hanifah Formation, and the Jubaila Limestone, with reported thicknesses of 184 m, 128 m and 116 m in Ar Riyadh area, respectively (Vaslet et al., 1991) (Fig. 6). The Jubaylah Limestone is conformably overlain by four depositional cycles, each comprising a lower carbonate unit and an upper anhydrite unit. The three older carbonate-anhydrite cycles plus the uppermost carbonate unit correspond to the Arab Formation, whereas the younger and thicker

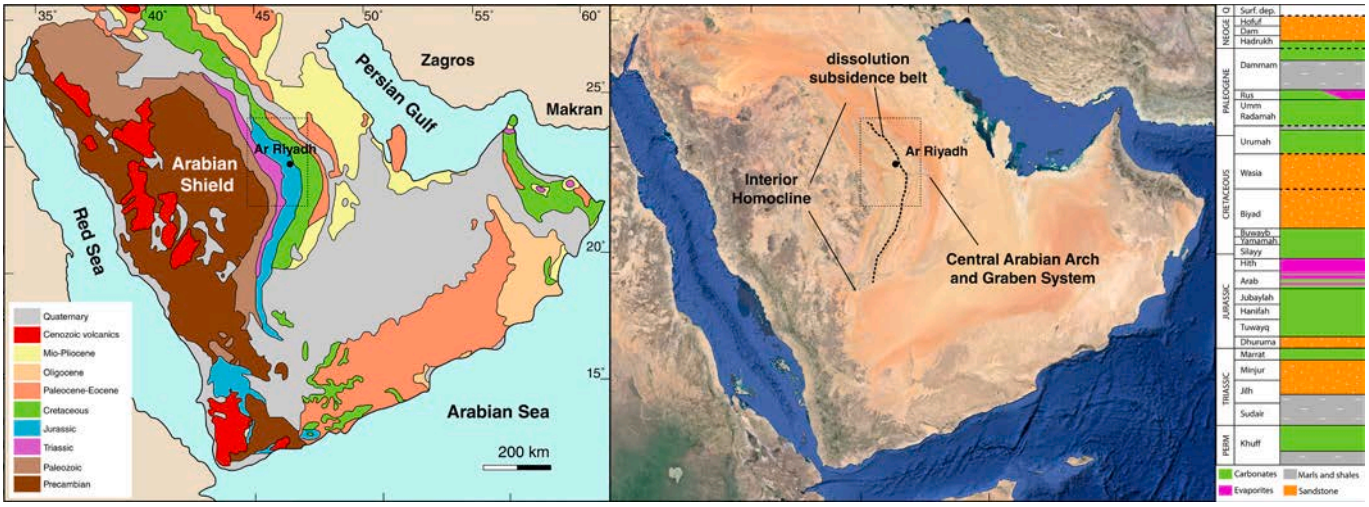

Fig. 6. Geological sketch and satellite image of the Arabian Peninsula and simplified lithostratigraphic section of the Arabian Platform in the Ar Riyadh region. Geological sketch from Pollastro et al. (1988) and Lindsay et al. (2006) and stratigraphic section adapted from Powers et al. (1966) and Rausch et al. (2014a, 2014b). The Late Jurassic Hith anhydrite aquiclude separates the Lower and Upper Mega Aquifer Systems. Satellite image downloaded from Google Earth. Inset polygon indicates location of Fig. 7.

anhydrite constitutes the Hith Formation. The Arab Formation is divided into four members, designated as A to D in descending order. Arab-A member refers to the upper carbonate unit, while B to D members include the successive carbonate-anhydrite couplets (Steineke et al., 1958a, 1958b). These formations, the thickness of which show a general decrease to the east, accumulated under arid conditions in a west-tilting intrashelf basin partially confined by a barrier along the east, which controlled the connectivity to the Neo-Tethys Ocean (Wilson, 2020). When the barrier was flooded, carbonates precipitated, and when the barrier was effective gypsum-anhydrite precipitated in supratidal sabkha and saline environments, closing the shoaling depositional cycle (Alsharhan and Kendall, 1994; Lindsay et al., 2006; Al-Mojel et al., 2020; Wilson, 2020; Wolpert et al., 2024). An exceptional exposure of the upper 90 m of the Hith Formation occurs SE of Ar Riyadh in the Dahl Hit sinkhole and cavern, described below (Powers, 1968; Powers et al., 1966; Wolpert et al., 2024 and references therein). The Hith Formation consists of anhydrite, mostly nodular (sabkha) and laminated (salina) facies, with some interbedded halite and carbonate layers. The carbonate beds are more abundant in the lower and upper parts of the Hith Formation, informally designated as the Rimthan and Manifa reservoirs, respectively (Powers, 1968; Sharief et al., 1991).

The Hith Formation is conformably overlain by limestone of the Upper Jurassic-Lower Cretaceous Silayy Formation, 110 m thick in Ar Riyadh area (Powers et al., 1966; Powers, 1968; Vaslet et al., 1991; Wolpert et al., 2015) (Fig. 6). The overlying Cretaceous succession includes the following units in ascending order (thicknesses reported by Vaslet et al., 1991 in the Ar Riyadh area): Yamamah Formation (limestone and calcarenite, 57 m), Buwayb Formation (limestone, 45 m), Biyad Sandstone (400 m), Wasia Formation (friable sandstone and claystone, 42 m), and Urumah Group (limestone, 176 m). The base of the Wasia Formation is a major erosional disconformity cut into progressively older formations towards the north, which involves a decrease in the stratigraphic thickness between the top of the Hith Formation and the base of the Wasia Formation, and locally the partial or total erosional removal of the anhydrite of the Hith and Arab formations (e.g., Vaslet et al., 1988; Memesh et al., 2012). The Urumah Group is conformably overlain by carbonate rocks of the Cenozoic Umm Radamah Formation. An additional formation is confined to the subsidence belt west of the dissolution front of the Hith Formation, designated as the Umm Sha'al formation (Vaslet et al., 1991). The Umm Sha'al formation, ca. 140 m thick in the Ar Riyadh area and of probable late Neogene to early Pleistocene age, consists of lithified alluvium, lacustrine-palustrine limestone and gypsum. It represents the oldest exposed infill of the subsidence trough created by the interstratal dissolution of the Upper Jurassic anhydrites. The Umm Sha'al formation typically shows a general dip towards the axis of the dissolution basin (Vaslet et al., 1991; Memesh et al., 2010).

In the Abu Jifan oil field (100 km east of Ar Riyadh), where the Arab and Hith anhydrites remain unaffected by any significant dissolution, the Arab and the Hith formations have an aggregate thickness of 326 m, of which 235 m correspond to the anhydrite units of Arab-D (36 m), Arab-C (40 m), Arab-B (27 m), and Hith Formation (132 m) (Vaslet et al., 1991). The carbonate units of Arab-D and Arab-C have considerable thickness (36 m and 45 m, respectively), while those of Arab-B and Arab-A are just 6 m and 4 m thick, respectively. West of the dissolution front of the anhydrite units, the thickness of the stratigraphic succession has been substantially reduced by the interstratal dissolution of the evaporites. The carbonate unit of the Arab-D overlying the Jubaylah Limestone remains essentially undisturbed, whereas the carbonate units originally underlain by the now dissolved evaporites have experienced subsidence and intense gravitational deformation, expressed by brecciation as well as complex sagging and collapse structures (Vaslet et al., 1991; Sharief et al., 1991; Memesh et al., 2008) (Fig. 8). Sharief et al. (1991), based on a stratigraphic correlation panel constructed with well logs and borehole data in the Ar Riyadh area, indicate that west of the dissolution front the thickness of the Hith Formation has been reduced from ca. 150 m to some 28 m of carbonates, essentially corresponding to the Rimthan and Manifa intra-Hith carbonate-rich reservoirs.

Two Mega Aquifer Systems separated by the Hith anhydrite aquiclude are differentiated in the hydrostratigraphy of the Arabian Platform, each comprising several aquifers separated by aquitards that locally have relatively higher vertical conductivity (Kalbus et al., 2011; Fuest et al., 2012; Rausch and Dirks, 2024) (Fig. 6): (1) the Lower Mega Aquifer System includes five major aquifers: Khuff (carbonates Upper Permian), Jilh-Minjur (sandstone, Triassic), Dhuruma (sandstone, Jurassic), and Arab (carbonates, Jurassic); and (2) the Upper Mega Aquifer System, composed of several aquifers in Cretaceous-Tertiary formations, notably the Biyad-Wasia sandstone aquifer and the Umm Radamah-Dammam karstified limestones. The Upper Mega Aquifer System is one of the largest aquifers in the world (ca. 1,860,000 km^2). The general groundwater flow direction follows the regional NE to E dip of the formations towards the Persian Gulf. The Hith anhydrite aquiclude east of its dissolution front prevents upward cross-formational flows to the upper aquifer system from the lower confined aquifer

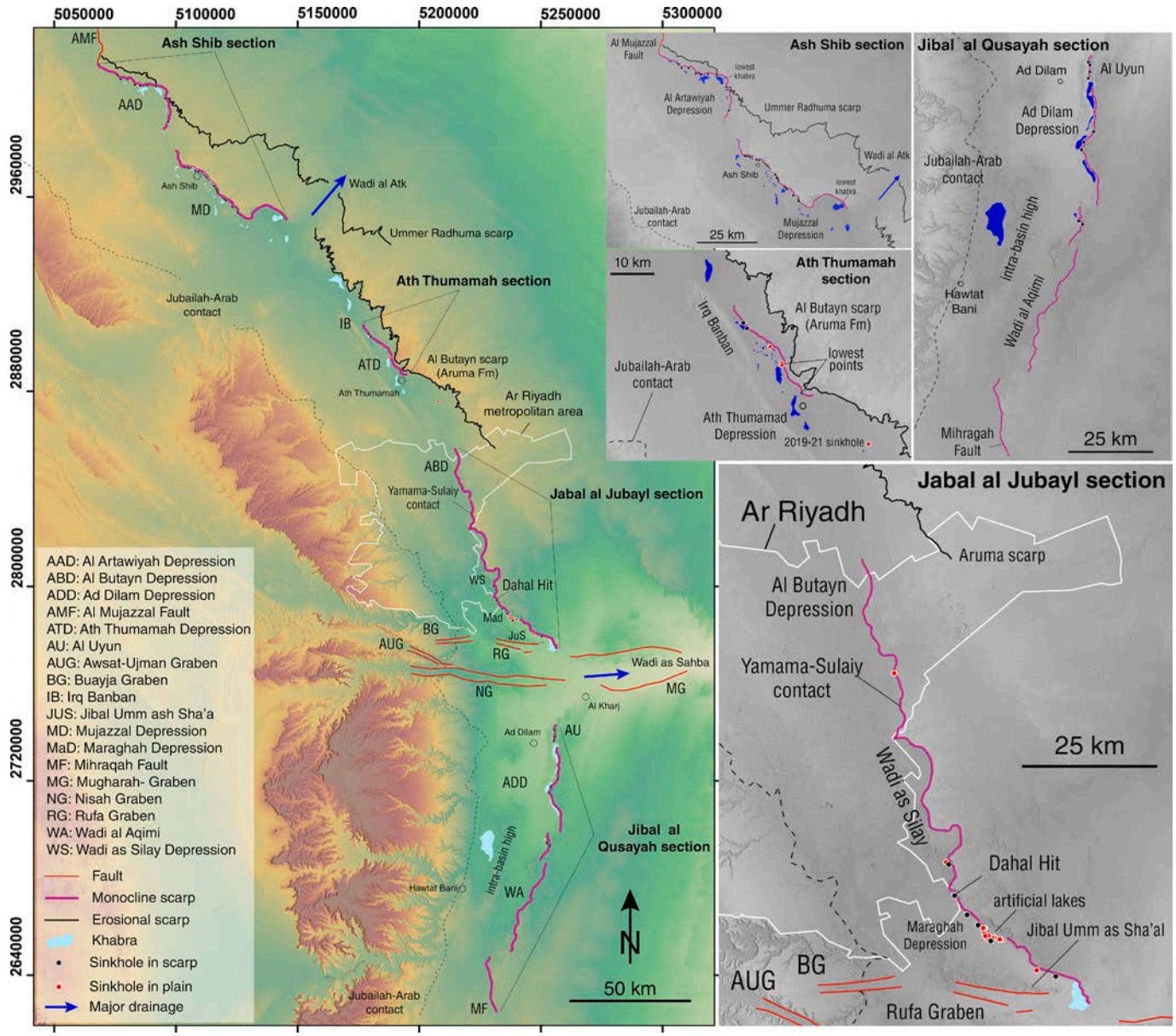

Fig. 7. General map of the discontinuous, W-facing, monoclinal fold scarp associated with the dissolution front of the Arab and Hith anhydrites and excerpts of the four sections of the fold scarp showing the distribution of the associated sinkholes and khabras (i.e., flat-floored depressions and ephemeral lakes). Relief models generated with 12 m resolution TanDEM-X DEMs.

system, which typically has higher piezometric heads. East-flowing transverse wadis cutting across the Jurassic succession bypass the Hith aquiclude, connecting the Lower and Upper Mega Aquifer Systems via Quaternary alluvium (Rausch and Dirks, 2024). The stored groundwater in both aquifer systems is mostly fossil water recharged during late Pleistocene and early Holocene pluvial periods. It is estimated the average annual precipitation during the "Pluvial Period" (9.5–5 ka) was around 350–450 mm/yr (Rausch and Dirks, 2024 and references therein). Currently, aquifers in Saudi Arabia have an overall natural negative water budget (greater discharge than recharge) related to the arid climate (<100 mm/yr), which in many regions is strongly aggravated by groundwater withdrawal, mainly for agriculture (Youssef et al., 2020; Rausch and Dirks, 2024).

4. Methodology

Mapping of the northern 420 km long section of the subsidence belt related to interstratal dissolution of the Arab and Hith evaporites, with especial focus on the monoclinal scarp atop the dissolution front and the associated sinkholes and surface ruptures, was carried out with ArcGISpro using the following spatial data: (1) 1:250,000 scale geological maps of the Saudi Geological Survey (Vaslet et al., 1988, 1991; Memesh et al., 2010, 2011, 2012); (2) satellite images available at Google Earth and ESRI World Imagery; and (3) TanDEM-X DEMs (German Aerospace Centre, DLR) and derived relief models with a spatial resolution of 12 m. The historical imagery of Google Earth was used to constrain bracketing ages for some recent sinkholes. Morphometric parameters were extracted using various tools of ArcGISpro and the TanDEM-X DEMs. These DEMs are derived from bistatic X-Band interferometric SAR data acquired by the satellites TanDEM-X (TDX) and TerraSAR-X (TSX). Elevations are defined with respect to the reflective surface of X-Band interferometric SAR returns. This implies, together with the sparse vegetation of the study area (ca. 100–200 mm/yr average precipitation), that the used DEMs essentially represent Digital Surface Models. TanDEM-X DEMs use the WGS84 datum and have a nominal pixel spacing of 12 m, absolute vertical accuracies of <10 m (90 % confidence

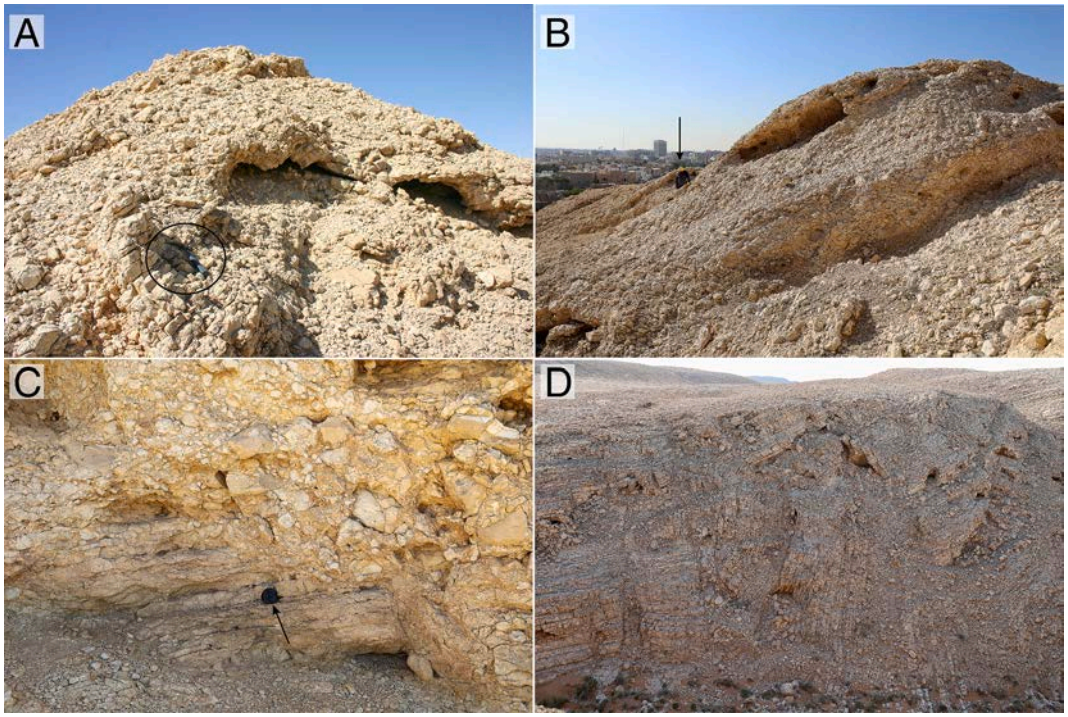

Fig. 8. Outcrops showing dissolution-collapse breccias and complex folding and collapse structures related to interstratal dissolution of anhydrite and gravitational deformation of overlying carbonate units. A: Hill underlain by a chaotic packbreccia on Arab-B in the Hawtat Bani Tamin quadrangle. Hammer for scale. B: Hill in Ar Riyadh city (Abu Makhroop; 38R 674592E 2,729,850 N) on the upper breccia complex (Arab-B, −A, Hith and lower part of Silayy). Arrow points to a person for scale. C: Close-up view of the chaotic and heterometric packbreccia in the site shown in B, including meter-scale clasts that preserve the original bedding. Lens cap 8 cm in diameter for scale. D: Intricate gravitational folding and collapse faulting affecting the well-bedded Silayy limestone on the northern margin of the Rufa Graben (38R 710039E 2,694,308 N).

interval), and a relative vertical accuracy of 2–4 cm (90 % confidence interval) (Wessel, 2016). Two water samples collected at Dahl Hit Cavern in November 2019 were analysed at the Chemical and Physical Analysis Unit of the Saudi Geological Survey and saturation indexes (SI) calculated with the PHREEQC code (Parkhurst and Appelo, 2013) and using the WATEQ4F database of thermodynamic data. Field work was conducted to examine the different sections of the subsidence belt with the aid of satellite images uploaded in a tablet with a GPS sensor and an UAV. For the names of the stratigraphic units we have used the nomenclature recommended by the Saudi Geological Survey (SGS, 2021).

5. General features of the monoclinal fold scarp atop the dissolution front of the Hith Formation

The monoclinal scarp developed over the dissolution front of the Hith anhydrite extends discontinuously for about 420 km, comprising around 300 km and 120 km long sections N and S of Al Kharj (Wadi as Shaba), respectively (Fig. 7). The drape-fold scarp, affected by abundant extensional surface ruptures (e.g., fissures, faults, grabens) and punctured by numerous sinkholes (Fig. 9), can be divided into four sections separated by gaps where the dissolution front and the associated monocline lack geomorphic expression. The Ash Shib, Ath Thumamah and Jabal al Jubayl sections are located N of Al Kharj, and the subsidence depression west of the Jabal al Jubayl escarpment hosts Ar Riyadh city. The Jibal al Qusayah section is located south of Al Kharj. The subsidence belt related to the interstratal dissolution of the Upper Jurassic anhydrites extends further to the SSW for 385 km to the As Sulayyil area, where the Mesozoic succession is concealed by the sands of the Rub' al Khali. In this southern sector sedimentary units affected by dissolution subsidence display extensive gravitational deformation, basin and dome morphostructure, sinkholes and poorly integrated and internal surface drainage, but there is not a clear monoclinal fold scarp defining the eastern boundary of the dissolution front (Kempe and Dirks, 2008; Dini et al., 2009).

5.1. Ash Shib scarp and the Al Artawiyah and Mujazzal depressions

This is a 118 km long, NW-SE oriented scarp section with a 9.6 km long gap (Fig. 7). In this sector of the Interior Homocline, the pre-Wasia unconformity has cut into Lower Cretaceous and Upper Jurassic formations, removing a progressively thicker succession towards the NW. According to the geological maps, in the NW sector of the scarp the exposed base of the Wasia sandstone lies on the Arab Formation (Al Artawiyah Quadrangle; Memesh et al., 2012), while in the SW zone the Wasia Formation is underlain by the Silayy Formation (Shaqra Quadrangle; Vaslet et al., 1988). This implies the complete erosional removal of the Biyad, Buwayb and Yamamah formations, in descending order, and the local, complete or partial removal of the Silayy, Hith and Arab formations. Because of the variable stratigraphic extent of the erosional hiatus, the remaining thickness of the evaporites of the Arab and Hith increases towards the SE, which entails greater dissolution and subsidence in the same direction.

In this section, the SW-facing monoclinal scarp is underlain by carbonate rocks of the Urumah Group (Fig. 9), and subsidence involves the Urumah Group and the Wasia and Silayy formations, plus units of the Hith and Arab formations that used to be underlain by anhydrite, now largely dissolved. In an embayment at the NW section of the scarp, the Umm Radamah Formation is most probably also affected by subsidence (Memesh et al., 2012). Here, the erosional scarp on the Umm Radamah Formation merges with the fold scarp (Memesh et al., 2012). The thickness of the downthrown sedimentary package varies from around 100 m in the NW to approximately 300 m in the SE, where the Silayy Formation may reach 150 m in thickness (Vaslet et al., 1988; Memesh

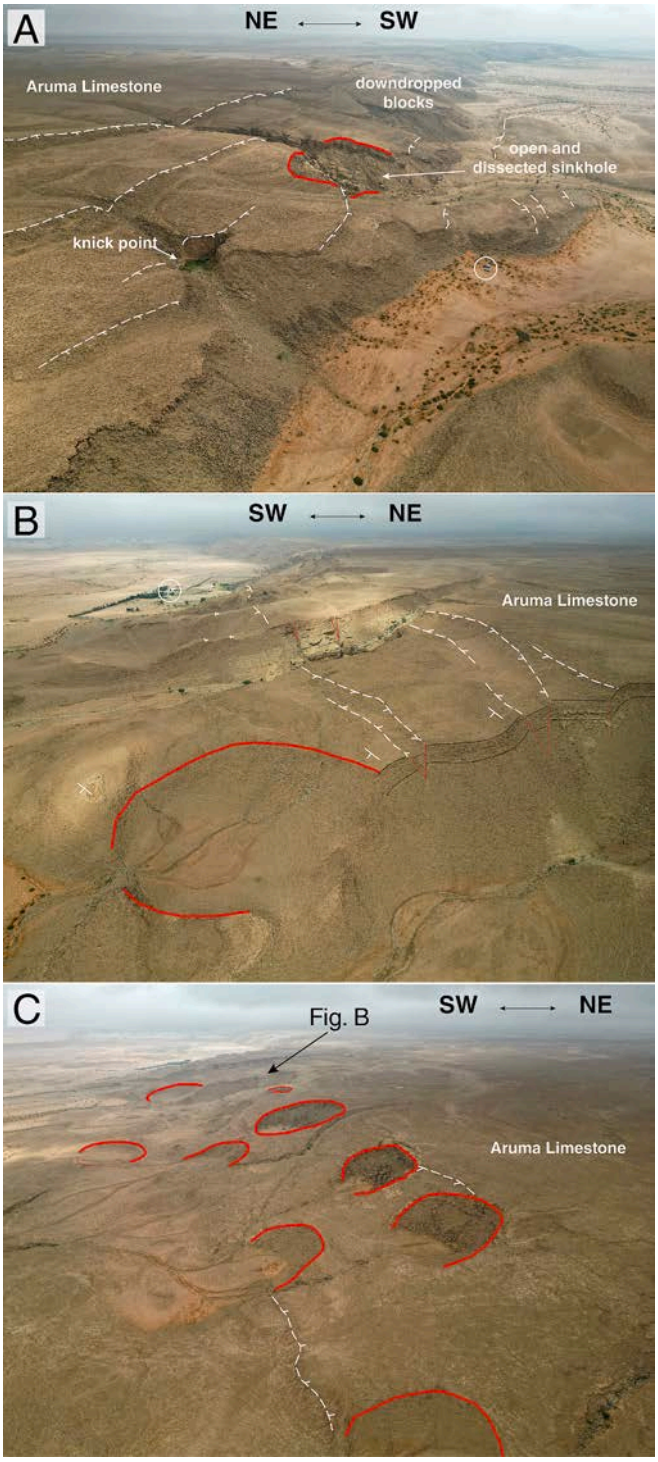

Fig. 9. Images of the Ash Shib section of the monoclinal scarp on Urumah Group SE of Ash Shib village. A: Monoclincal fold scarp with synthetic normal fault scarps and an open caprock collapse sinkhole. Knick point in a transverse downdip drainage associated with a fault scarp. Inlier of collapsed Urumah limestone in the piedmont with preserved fault scarps. Cars marked with a circle for scale. B: Articulated monocline with normal faults and keystone grabens. Dissected caprock collapse sinkholes in the foreground. House marked with a circle in the background for scale. C: Monoclinal fold scarp punctured by numerous large caprock collapse sinkholes, showing a higher degree of degradation and integration into the drainage network towards the foot of the scarp. Sinkholes associated with the crest of the monocline are 100–140 m across.

et al., 2012). In the southern sector, Vaslet et al. (1988) reports the dissolution of around 100 m of evaporites, subsidence of a similar magnitude in the overlying sediments, and the transformation of the Arab and Hith formations (excluding the limestone unit of Arab D) into a residual dissolution-collapse breccia around 55 m thick.

The monoclinal scarp is underlain by the Upper Cretaceous Urumah Group, consisting of carbonate rocks with interbedded shales (Khinsar, Hiqaqah, Linah formations in ascending order) (Fig. 9). The dissolution-induced fold is situated at a distance of around 50 to 30 km NW from the exposure of the Jubaylah-Arab contact, showing a general decrease towards the SE. This suggests progressively greater propagation of the dissolution front towards the NW, where the evaporites have lower thickness. Interstratal dissolution has generated a 100 km long subsidence trough west of the monoclinal scarp known as the Al Artawiyah depression (Al Artawiyah Quadrangle) and the Mujazzal depression (Shaqra Quadrangle), which form part of the ca. 220 km long Al Butayn depression that extends up to Ar Riyadh. The infill of the subsidence basin includes lithified alluvium and lacustrine limestone and gypsum of the Umm Sha'al formation (Vaslet et al., 1991) with a poorly constrained late Neogene-Pleistocene age (Vaslet et al., 1988; Memesh et al., 2012), plus widespread unconsolidated Quaternary deposits of variable nature (alluvial, eolian, lacustrine). To the east of the monoclinal scarp the landscape is dominated by extensive dipslopes underlain by carbonate rocks of the Urumah and Umm Radamah limestones, gently dipping to the NE and the latter forming the Al Arumah plateau.

The scarp displays a relatively sinuous trace with a 9.6 km long gap where the monocline is concealed by Quaternary deposits (Fig. 7). The aggregate cartographic length of the scarp of 118 km (51,1 and 66.9 km) and the straight length of 92,8 km measured as a rectilinear distance between the tips of the segments (38.6 and 54,2 km) indicate a sinuosity index of 1.27. The northern termination of the scarp is probably controlled by the disappearance of the Arab and Hith evaporites related to the pre-Wasia erosional unconformity, which cuts into progressively older units towards the north, and the presence of the N-S oriented and W-verging Al Mujazzal Fault (Memesh et al., 2012). The southern termination of the scarp section occurs at Wadi al Atk, a major NE-flowing transverse drainage that dissects the Al Arumah plateau at the Udayniyat water gap. To the SE the monoclinal fold is concealed by Quaternary deposits and the deformational scarp is replaced by a highly digitated erosional scarp at the front of a cuesta capped by limestone of the Urumah Group overlying the friable Wasia sandstone. In this sector, the erosional recession of the scarp and the associated high sediment yield have outpaced both the lateral migration of the dissolution front and the accommodation space created by subsidence, burying the monoclinal fold. The more rapid scarp retreat can be attributed to the nature of the escarpment, including highly erodible Wasia sandstone. The Wasia sandstone is rapidly eroded by headward propagating gullies, leading to the undermining and collapse of the caprock made up of Urumah limestone.

The sinuous monoclinal scarp shows two embayments 20 and 9 km long where the dissolution front has advanced around 8 and 11 km further to the NE. In the northern embayment, the trace of the monoclinal scarp coincides with the erosional scarp of the cuesta developed on the Paleocene-Eocene limestone of the Umm Radamah Formation, forming a compound scarp (deformational and erosional) (38R 5777626E 2,897,661 N). In the central sector the Ash Shib scarp shows a salient 8 km long and 3.5 km wide (strike-normal) associated with a sharp change in the scarp trend. Here, the greater development of extensional structures can be ascribed to limited lateral confinement of the rocks in the salient, where fissures have been transformed into deep scarp-parallel valleys (38R 58227E 2,869,645 N).

The limestone outcrops of the Urumah Group associated with the 6 km long northernmost section of the scarp display a striking concordant hummocky topography underlain by a basin and dome structure, attributable to differential interestratal dissolution and subsidence. A significant proportion of the dome-shaped hills show a crater-like,

closed and open depressions at the summit attributable to collapse processes and/or differential erosion (Fig. 10). Extensional morphostructures look rather degraded in this section of the monoclinal scarp, except along the ca. 30 km long segment associated with Ash Shib village. Here, the escarpment around 100 m high shows a very prominent geomorphic expression with fresh-looking fault scarps and grabens and a very high density of caprock collapse sinkholes, locally offset by faults (Fig. 11A). This evidence suggests active, more active, and/or relatively more recent interstratal dissolution and subsidence. Locally, at the foot of the scarp (lower limb of the monocline), there are inliers of collapsed Urumah Group not buried by Quaternary deposits that show longitudinal antislope scarps and serrated topography (ridges and troughs) inherited from extensional structures developed when the rocks where located at the crest of the monoclinal scarp (Fig. 9A).

The drainage in the Al Artawiyah and Mujazzal depressions is largely deranged and discontinuous. The satellite images and the DEMs reveal a dominant SE-directed strike (subsequent) paleodrainage, expressed as discontinuous sections of dry wadis and khabras. The elevation of the khabras and the paleodraiange sections decrease progressively to the SE. These paleodrainages connects with the transverse N*E*-directed Wadi al Atk at the SE termination of the monoclinal scarp. Some khabras may correspond to subsidence basins. At the foot of the scarp some sinkholes host ephemeral water-table lakes that function as inlet points for local drainage networks. Some NE flowing valleys carved in the plateau east of the scarp (e.g., Wadi Qurayy) display heads truncated at the monoclinal scarp and valley sections with reversed SW-directed gradients, revealing the beheading of drainage by the NE recession of the monoclinal scarp related to the long-term migration of the dissolution front (38R 596796E 2,860,817 N).

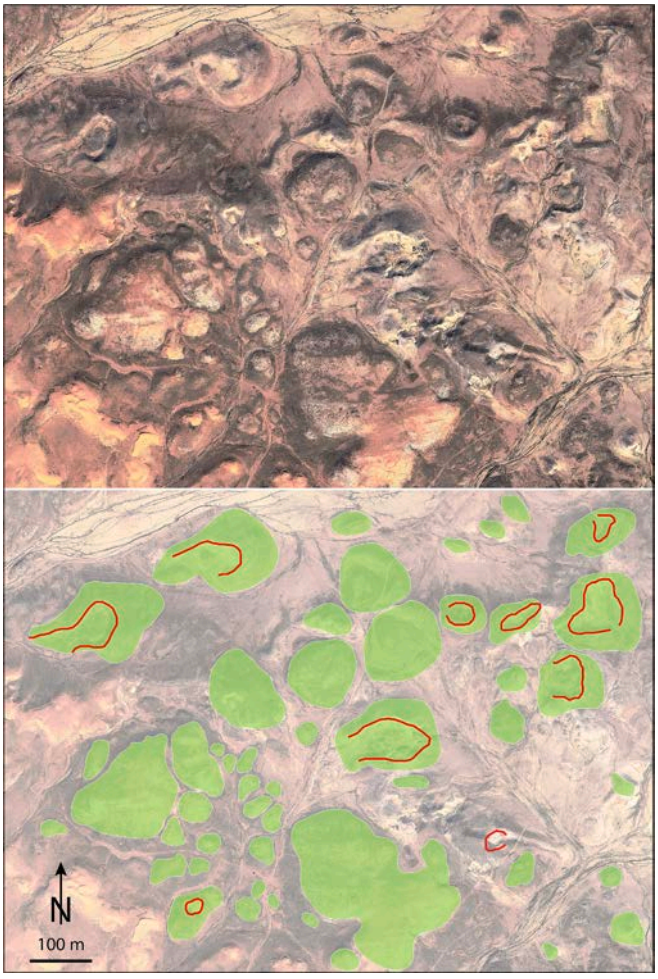

Fig. 10. Hummocky topography associated with the northernmost sector of the Ash Shib scarp underlain by a basin and dome structure related to differential interstratal dissolution and subsidence. Note crater-like depressions, both enclosed and open, attributable to collapse at the crest of some hills.

5.2. *The Ath Thumamah scarp and depression*

This is a 30.2 km long scarp section with NW-SE orientation associated with the Ath Thumamah depression (Fig. 12). In this sector, erosion preceding the deposition of the Upper Cretaceous Wasia sandstone removed the Biyad Formation, thus the Wasia Formation unconformably overlies the Buwayb Formation (Memesh et al., 2011). The monoclinal fold scarp is underlain by carbonate rocks with shales of the Lower Cretaceous Yamamah Formation (28 m thick) and Buwayb Formation (18 m thick). Here, subsidence has also affected the Silayy (103 m thick), the Hith and the Arab formations. The foundered sediments overlying the Hith Formation have an aggregate thickness of 149 m (Memesh et al., 2011). The dissolution-induced fold is situated around 35 km to the NE of the Jubaylah-Arab contact, providing a minimum estimate for the lateral migration of the evaporite-dissolution and subsidence phenomena. Here, the 20 km wide and strike-parallel subsidence trough located west of the monoclinal scarp is known as the Ath Thumamah depression, which hosts the longitudinal erg Irq Banban. In the subsidence belt located west of the dissolution front, the Arab and Hith formations have been largely reduced to a residual condensed sequence mainly consisting of collapse breccias. The Silayy limestone is affected by intense gravitational deformation, including brecciation and folding related to differential interstratal dissolution and subsidence (passive bending). Breccias dominate in the lower section of the formation, while complex multidirectional folding and basin and dome structures are more common in the upper part of the formation (Memesh et al., 2011). The foundered Mesozoic bedrock in the deeper portion of the Ath Thumamah depression is covered unconformably by the late Neogene-Pleistocene Umm Sha'al formation and extensive unconsolidated Quaternary deposits accumulated in diverse environments (alluvial fans, wadis, sand dunes and sheets, khabras).

The Ath Thumamah fold scarp ca. 80 m high shows a relatively straight trace with a cartographic length of 30.2 km and a straight length between the tips of 27.7 km, yielding a low sinuosity index of 1.1. The trace of the scarp shows broad west-facing convexities and concavities and in the southern sector a sharp change in direction, from N-S to E-W, forming a salient where the scarps and fissures show intersecting nearly orthogonal directions. In the large gaps to the NW (52 km long; between the Ash Shib and the Ath Thumamah sections) and to the SE (36 km long; between the Ath Thumamah and Jabal al Jubayl sections), the drape fold atop the dissolution front is buried by Quaternary deposits. The burial of the scarp is favoured by the presence of the high-relief Al Butayn escarpment to the west, capped by the Urumah Group. The distance between the fold scarp and the highly digitated erosional scarp at higher elevation varies from 0.8 km in the southern sector (compound scarp) to around 9 km in the northern sector. The high sediment yield from the rapidly retreating erosional Al Butayn escarpment towards the dissolution-induced basin seems to overwhelm the accommodation space created by subsidence, burying the fold. The location of the concealed dissolution front and monocline is probably indicated by a recent large cover and caprock collapse sinkhole (volume $> 40{,}000\ m^3$) that lies at the southeastward projection of the fold scarp (38R 679611E 2,782,485 N; Fig. 13).

The extensional structures associated with the crest of the monocline show a general degraded appearance, except along a 1.5 km long outwardly convex stretch where the upper hinge and intermediate limb of the fold are ruptured by fresh looking grabens, faults scarps and fissures that locally disrupt drainages (Fig. 12). In the northern sector the scarp is scalloped by two coalesced and open caprock collapse sinkholes with an aggregate length of 619 m (Fig. 11C). An extensional structure connected with an entrenched drainage that traverses the scarp has been

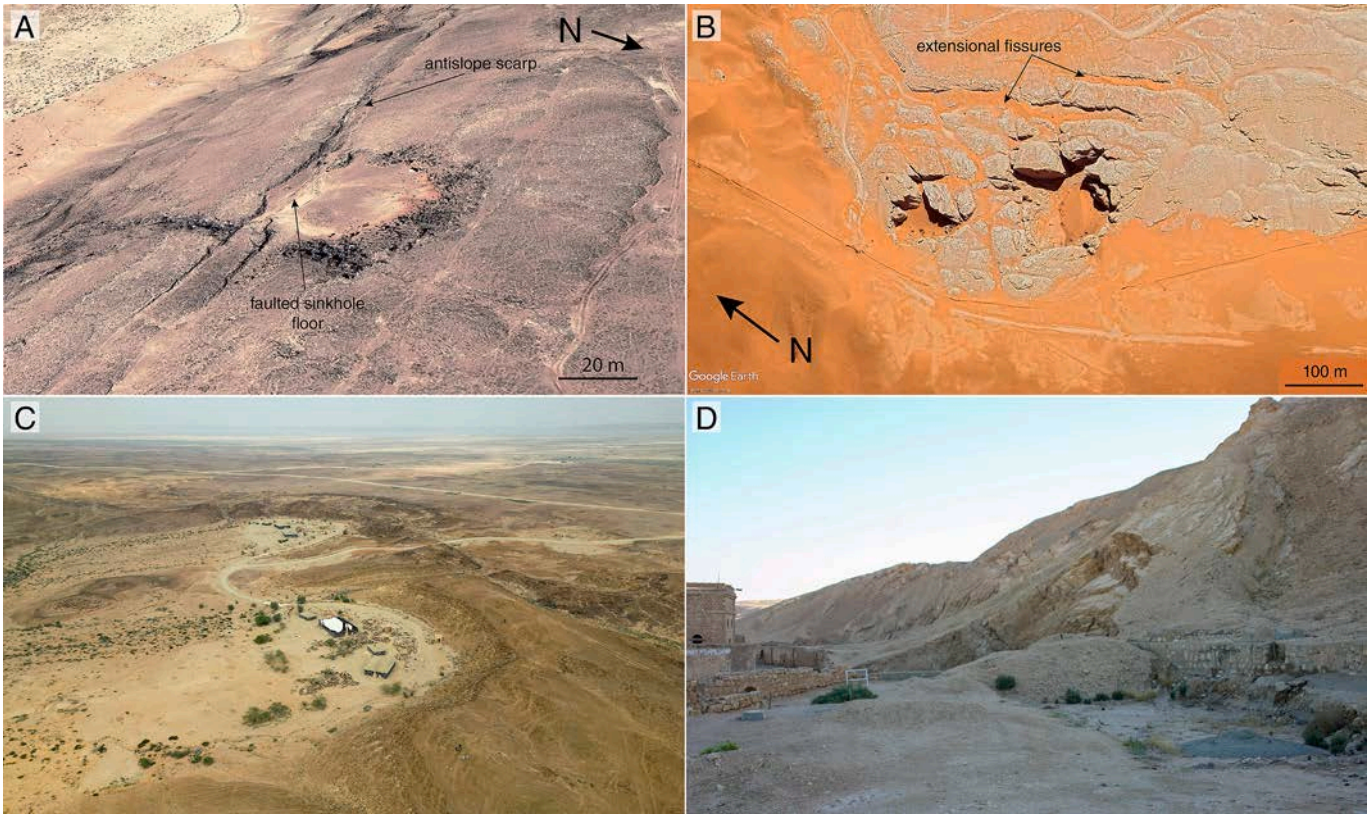

Fig. 11. Examples of caprock collapse sinkholes associated with the monoclinal scarp. A: Sinkhole in the Ash Shib scarp section on Urumah Group, the floor of which is offset by an antithetic fault, expressed as an antislope scarp (38R 587216E 2,868,800 N). B: Two adjacent steep-sided sinkholes in the Jibal al Qusayah section on Silayy limestone associated with large-separation fissures and showing a polygonal geometry. Corridor-like fissures and sinkholes largely filled by eolian sand (38R 724675E 2,661,105 N). C: Compound open sinkhole 619 m long related to the coalescence of two adjoining sinkholes in the Ath Thumamah scarp section on Yamamah Formation (38R 653504E 2,807,783 N). D: Sinkhole used for water supply at Al Khafs in the Jibal al Qusayah on Silayy limestone (38Q 723311E 2,637,625 N). Images A and B captured from Google Earth.

transformed into a striking narrow and rectilinear canyon 375 m long (38R 663585E 2,795,467 N). Some sinkholes (locally know as dahls, duhuls) at the foot of the scarp host ephemeral lakes and collect runoff from centripetal drainage networks. The Ath Thumamah depression shows a general NW-directed paleodrainage towards Wadi al Atk, but has been distorted by subsidence and re-routed towards some sinkholes at the foot of the scarp, some of which host ephemeral lakes.

5.3. *The Jabal al Jubayl scarp in the Ar Riyadh area*

The Jabal al Jubayl escarpment, 116.4 km long and east of Ar Riyadh, has a NW-SE trend that veers to a WNW-ESE orientation in the southern portion. In this section the monoclinal scarp is developed on limestone of the Upper Jurassic-Lower Cretaceous Silayy Formation, except in the northern sector where the carbonate rocks exposed correspond to the overlying Lower Cretaceous Yamamah Formation (Figs. 14, 15, 16). The formations affected by dissolution-induced subsidence include, in addition to the Arab and Hith, the Silayy, Yamamah and Buwayb formations. The aggregate thickness of the collapsed units overlying the Hith Formation is around 212 m (Vaslet et al., 1991).

The Dahl Hit cavern (38R 702378E, 2,709,459 N), also known as Ayn Hith (dahl = sinkhole; ayn = spring in Arabic), associated with a caprock collapse sinkhole at the foot of the scarp, offers the best outcrop of the Hith Formation, with the upper 90 m exposed (Vaslet et al., 1991; Wolpert et al., 2024) (Fig. 17). In 2010, Wolpert et al. (2024) logged the lowermost 28.5 m interval in the bottom of the cavern, documenting the vertical stacking of saline (subaqueous) and sabkha (subaerial) facies that record transgressive-regressive cycles. The contact between the Hith and Silayy formations is observable at the entrance of the cavern. Here, well and thinly stratified anhydrite in the upper part of the Hith Formation shows two intercalated beds of fine-grained material with matrix-supported angular carbonate clasts (Fig. 18). These beds 1–3 m thick correspond to dissolution residues and matrix-supported collapse breccias (i.e., floatbreccia) related to interstratal evaporite dissolution and the collapse of interbedded and overlying carbonate layers, leaving the remaining non-soluble fraction of the leached beds (breccias 1 and 2 of Wolpert et al., 2024). The base of the lower dissolution residue and breccia (labelled as DR and CB 1 in Fig. 18) locally displays a highly irregular geometry that penetrates into the underlying anhydrite truncating its layering. Some authors placed the base of the Silayy Formation at this contact, and interpreted it as an erosional unconformity (Steineke et al., 1958a, 1958b) or disconformity (Vaslet et al., 1991). However, its association with a dissolution residue and collapse breccia indicates that it corresponds to a secondary contact related to the uneven downward advance of a dissolution front into the underlying anhydrite (Powers et al., 1966; Powers, 1968; Wolpert et al., 2015, 2024). The more planar base of the upper dissolution residue and breccia (labelled as DR and CB 2 in Fig. 18) also truncates anhydrite beds, and the overlying anhydrite just below the Hith-Silayy boundary shows synforms and breccias attributable to interstratal dissolution and local ductile (sagging) and brittle subsidence (collapse).

Over several decades before 2010 the water level in the cave dropped around 100 m due to agricultural groundwater withdrawal (Kempe and Dirks, 2008). The largely fossil groundwater was pumped from wells tapping the underlying carbonate aquifer of the Arab Formation. Between 2010 and 2016, the water level rose by about 50 m. The change in the water table is attributed to the storage of treated sewage water in a former quarry 10 km to the SE and associated with the dissolution front

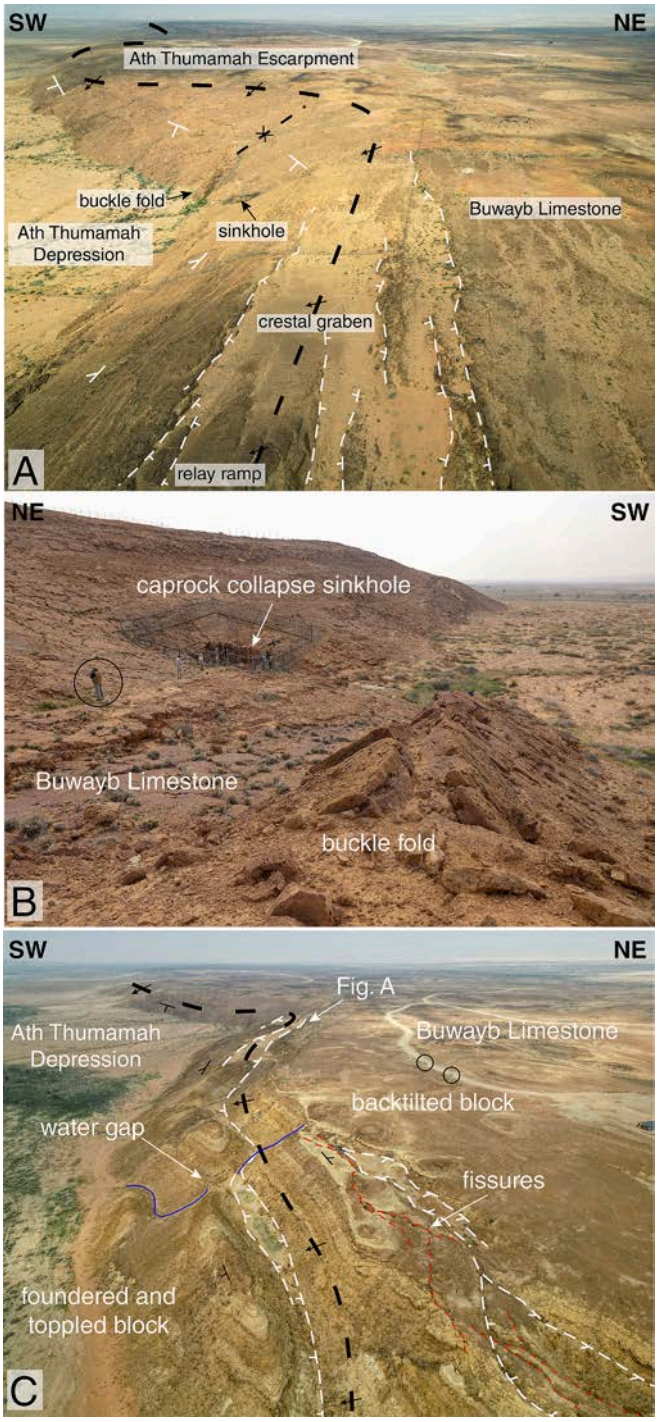

Fig. 12. Images of the Ath Thumamah escarpment affected by crestal extensional structures on the Buwayb Formation. A: Sinuous fold scarp with a crestal graben bounded by synthetic and antithetic faults with en echelon arrangement and associated accommodation ramps. B: Buckle fold with geomorphic expression related to inner-arch contraction in the transverse synclinal hinge associated with a sharp change in the monocline trend (see location in A). Fenced caprock sagging and collapse sinkhole in the lower part of the fold scarp. C: Crest of articulated monocline affected by a synthetic normal fault with associated keystone grabens and separating blocks with flat lying and forward tilted strata. Transverse drainage disrupted by normal faults and fragmented into a blocked section and a decapitated section above and below a water gap, respectively.

(38R 709293E 2,701,970 N) (Michelsen et al., 2016; Wolpert et al., 2024). According to historical imagery of Google Earth, the storage of water and thus the artificial aquifer recharge started sometime between May 17, 2009 and May 15, 2011. Michelsen et al. (2016) reconstructed a water level rise of 9.5 m over two years (January 2013–December 2014) using YouTube videos (social media mining), with a rather constant rate of 0.4 m per month and an acceleration (1.3 m/month) in the fall of 2013. Vaslet et al. (1991) also reported exposures of the Hith Formation in the walls of two adjacent collapse sinkholes located 3.9 km to the SE of Dahl Hit, at the foot of the Jabal al Jubayl escarpment (38R 704552E, 2,706,137 N; Fig. 14A).

On November 2019, two samples were collected from different points at the surface of the water-table lake in the bottom of the Dahl Hit Cave, providing similar results (Fig. 17D; Table 1). The chemistry of the waters, in direct contact with the Hith anhydrite, is consistent with its sulphate karst setting. The water is in equilibrium with anhydrite (SI -0.08), slightly supersaturated with respect to gypsum (SI 0.14), strongly undersaturated with respect to halite (SI -6.1), and slightly supersaturated with calcite (SI 0.2–0.4). The concentrations of sulphate (1950–1946 mg/L) and chloride (296–293 mg/L) indicate the dissolution of 2.75 g of anhydrite and 0.5 g of halite per litre of water, assuming that the totality the anions are derived those minerals. The relatively low Na and Cl concentrations are consistent with the limited halite content in the Arab and Hith formations (Vaslet et al., 1991), and probably also with their occurrence within low-permeability anhydrite beds. The Cl/Na molar ratio of 1.5 could be related to Ca—Na cation exchange processes, consistent with the SO_4/Ca ratio of 0.86 and sources for Cl additional to halite, likely related to the presence of other chloride salts in the Hith Formation. Interestingly, the water has anomalously high SiO_2 contents (69–83 mg/L) and is close to equilibrium with amorphous silica (SI –0.14 to −0.22). Given the lack of hydrothermal activity in the area, a potential source to be considered is the chemical treatment of the waste water stored in the nearby artificial lakes, although this issue remains uncertain. A water sample collected in 2003 at Dahl Hith by Gregory (2011) provided similar results to those presented in this work.

The propagation of the dissolution front and the accompanying subsidence has created an asymmetric elongated basin around 30 km wide flanked by the 100–130 m high Jabal al Jubayl escarpment on the NE margin and outcrops of Mesozoic carbonate rocks with gently inclined or hilly topography on the opposite side. The Jubaylah-Arab contact is situated at 15–30 km SW of the scarp. The subsidence trough, which hosts Ar Riyadh city with more than 8 million inhabitants, receives the following names from NW to SE (Fig. 7): (1) Al Butayn NW of Ar Riyadh; (2) Wadi as Silay in the Ar Riyadh area; and (3) Maraghah depression between Ar Riyadh and Wadi as Shaba. On the SE margin of the Maraghah depression and N of the Rufa Graben there is an extensive outcrop of the Umm Sha'al formation which unconformably overlies all previous formations at Jibal Umm ash Sha'al, the type locality of the formation (Vaslet et al., 1991). This formation forms part of the infill of the dissolution basin, is around 140 m thick, and consists of cemented alluvium (lacking clasts derived from the Arabian Shield) and lacustrine limestone and gypsum. The strata show a general NE dip of up to 30° decreasing towards the trough axis, and is unconformably overlain by younger unconsolidated Quaternary deposits in the lower part of the basin, showing an overall offlap arrangement (Vaslet et al., 1991) (Fig. 16). In this sector, Vaslet et al. (1991) also mapped the Rufa formation (Pleistocene?), up to 15 m thick consisting of cemented alluvium overlain by a caprock of limestone. This deposit unconformably overlies the Umm Sha'al and Mesozoic formations and occurs both within the subsidence trough and at the margins forming buttes and mesas.

The carbonate units of the Arab-C, —B, and -A members, and the lower part of the Silayy limestone have been largely transformed into a dissolution-collapse breccia. Vaslet et al. (1991) differentiated in their cartographic work into a lower breccia complex (Arab-D and —C) and an upper breccia complex (Arab-B, –A, Hith and lower part of Silayy). They observed higher clay content and larger clasts, including blocks tens of

Fig. 13. Expanding cover and bedrock collapse sinkhole 50 m long in the Ath Tumamah depression occurred between December 2017 and July 2019 and associated with a water pipe. The sinkhole is located at the SE projection of the Ath Thumamah fold scarp, suggesting its association with a buried dissolution front (38R 679611E 2,782,485 N).

meters long, in the upper breccia complex. Excellent exposures of the upper breccia can be observed in hills within Ar Riyadh city, such as at Abu Makhroop (38R 674592E 2,729,850 N; Fig. 8B, C). West of the dissolution front, the upper part of the Silayy limestone typically displays a complex multidirectional folded structure related to differential interstratal dissolution and passive bending (Fig. 8D). Locally, it shows a striking basin and dome morpho-structure, with domes showing centrifugal dips and basins centripetal (i.e., quaquaversal) dips. The summit of some domal hills exhibit circular depressions that may host remains of sediments that used to be situated at higher elevation (Yamamah Formation, Rufa formation), suggesting post-folding collapse (Fig. 19).

Fig. 16 shows a strike-normal schematic cross-section (x5 vertical exaggeration) illustrating the subsidence of the carbonate units of the Arab-C, —B, and –A members, and the Silayy Formation related to the complete dissolutional removal of the Arab and Hith anhydrites. The cross-section considers a 1° regional dip, the thickness indicated by Vaslet et al. (1991) for the non-disturbed units in Ar Riyadh area, and the thickness of the Arab and Hith formations (235 m) in the Abu Jifan oil field located 100 km east of Ar Riyadh. Moreover, it is constructed assuming that the anhydrite units have no insoluble content, and that the gravitational deformation and brecciation of the collapse units do not involve any volume increase (i.e., bulking effect). This cross-section shows a subsidence magnitude (i.e., throw) related to the interstratal evaporite dissolution of 235 m, which should be considered as a maximum estimate for the reasons indicated above. Vaslet et al. (1991), based on the thickness of the Umm Sha'al formation and the elevation of the Jabal al Jubayl scarp, estimated a cumulative subsidence of around 140 m, which should be considered as a minimum value.

In the southern sector of this section, the Umm Sha'al formation and previous formations are affected by both evaporite dissolution subsidence and tectonic subsidence related to the Central Arabian Graben System, with typical overall throws in the grabens of around 300 m. Vaslet et al. (1991) analysed the geometrical relationships between the different deformation structures in the Rufa Graben, inferring the following chronological sequence: (1) normal faulting of Mesozoic formations; (2) dissolution-induced subsidence affecting normal faults and controlling deposition of the Umm Sha'al formation; (3) renewed normal faulting that offset around 100 m the Umm Sha'al formation and locally also the younger Rufa formation, with 16 m throw in the Rufa Graben. This is a very special case in which two types of deformation with markedly different spatial-temporal patterns are superposed: (1) spatially stationary and deeply rooted tectonic faulting; and (2) laterally migrating deformation confined to the supra-evaporite units. Chronological relationships between the two types of deformation can show spatial variations, given the fact that interstratal dissolution and subsidence are laterally migrating processes.

The trace of the Jabal al Jubayl escarpment is relatively sinuous, with large embayments and sharp salients. The cartographic and straight lengths of the scarp are 116.4 km and 96.9 km, respectively, yielding a sinuosity index of 1.2. East of Ar Riyadh it shows a large embayment 12 km long and 4.5 km wide, the northern edge of which is marked by a pointed salient. To the SE of Ar Riyadh there is another embayment 6.5 km long and 4.5 km wide. These are sections where the dissolution front has experienced significantly greater NE advance. The Jabal al Jubayl scarp is interrupted N of Ar Riyadh, where the monoclinal scarp is buried by Quaternary deposits, largely comprising alluvium shed from an erosional scarp consisting of friable Wasia sandstone capped by Urumah limestone. The southern termination of the Jabal al Jubayl scarp is controlled by the Mugharah Graben and the associated *E*-flowing Wadi as Sahba (i.e., Al Kharj water gap). Wadi as Sahba is a major drainage flowing towards the Persian Gulf that has perched terraces with clasts sourced from the Arabian Shield (Vaslet et al., 1991). The subsidence trough SW of the Jabal al Jubayl scarp shows a general SE-directed drainage towards Wadi as Sahba through the Wadi as Silay, but this stream is interrupted in a poorly drained area around 5 km south of Dahl Hit sinkhole and cave. Khabras around Al Kharj indicate the presence of endorheic areas and disrupted drainage in the southern sector of the dissolution trough attributable to differential dissolution-induced subsidence (Vaslet et al., 1991). Evidence of recent subsidence is provided by deformation of recent alluvium exposed in quarries at the foot of the monoclinal scarp. A good example can be observed in the quarries just south of the Dahl Hit, where alluvial fan deposits are

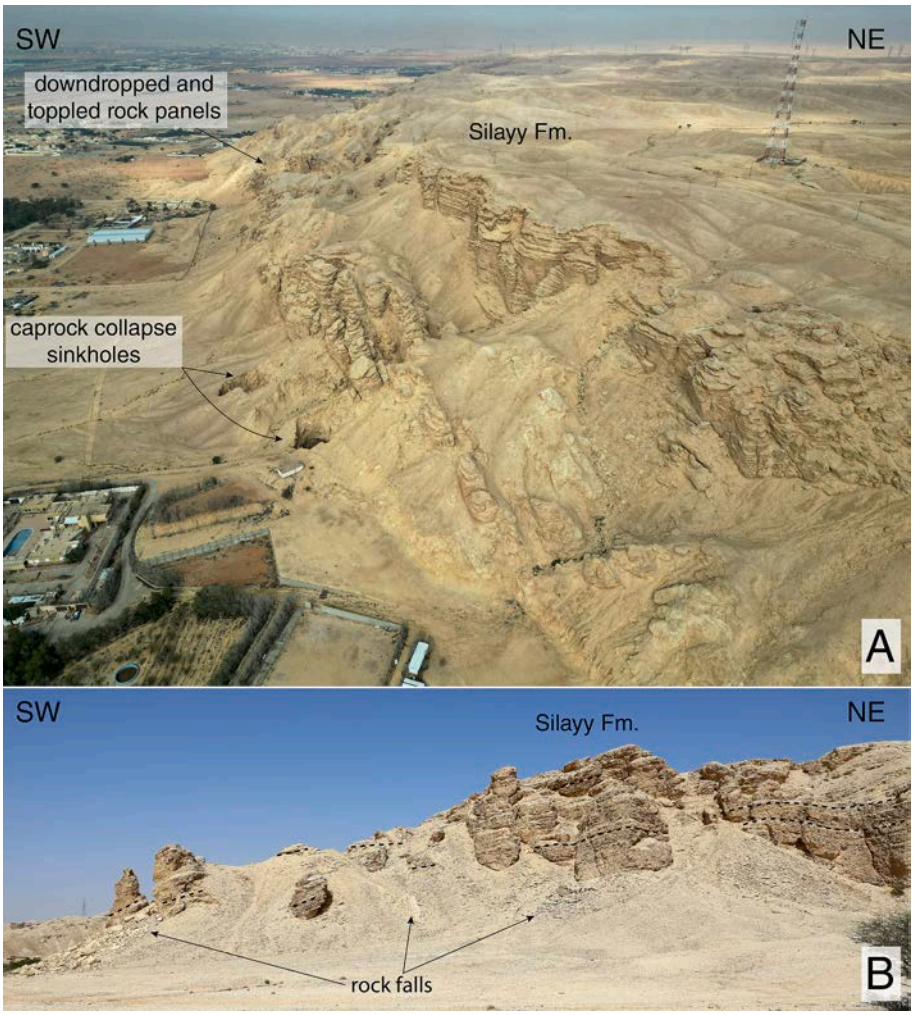

Fig. 14. Images of the Jabal al Jubayl escarpment south of Ar Riaydh. A: Foundered and toppled elongated blocks of Silayy limestone and two steep-sided caprock collapse sinkholes with exposures of the Hith Formation in their walls (38R 704552E, 2,706,137 N). B: Monoclinal fold scarp on strongly fractured Silayy limestone, largely covered by talus deposits.

tilted dipping towards the escarpment and show normal faults with centimetre- and decimetre-scale throws and dilated joints (Fig. 20). Note that the backtilted alluvium was accumulated in the piedmont with a low syndepositional dip away from the scarp.

5.4. *The Jibal al Qusayah scarp and the Ad Dilam depression*

The Jibal al Qusayah monoclinal scarp, at the eastern edge of the Ad Dilam depression, extends discontinuously along 129 km south of the Central Arabian Arch and Graben System (south of Al Kharj), were the Interior Homocline strikes NNE-SSW. This is the geometrically most complex section of the fold scarp, with step overs and gaps and in some sectors a difficult to map trace because of its low relief and erosional degradation (Fig. 7). In this section the fold scarp is underlain by the Silayy Formation (Fig. 11D), and dissolution-induced subsidence has affected, in addition to the Arab and Hith formations, the Silayy, Yamamah and Buwayb formations, with an aggregate thickness of 167 m (Memesh et al., 2008, 2010). Vaslet et al. (1991) reported three caprock collapse sinkholes in the Al Uyun area (Ayn ad Dilh, Samhah, and Umm Khisah) in which the Hith anhydrite is exposed and partially hydrated into gypsum. Subsidence related to interstratal dissolution of the anhydrite units has created the NNE-SSW-oriented and 20–30 km wide Ad Dilam subsidence basin west of the dissolution front, superposed on the regional ESE-dipping homoclinal structure. This is a compound morpho-structure consisting of two sediment-filled troughs and an intervening antiformal high, expressed as a large inlier of complexly deformed Silayy limestone. This structure suggests incomplete anhydrite dissolution beneath the intrabasin antiformal high revealing less subsidence. The collapsed formations display a wide variety of gravitational deformation structures, including stratiform and transtratal dissolution-collapse breccias and complex passive-bending folds with random strike and dips. The carbonate components of the Arab (C to A members) and the Hith and the lower part of the Silayy limestone formations have been largely transformed into a massive breccia (Fig. 8A). Memesh et al. (2010) measured a thickness of 85 m for the condensed and disrupted Arab Formation, the thickness of which is 143 m in the Abu Jifan oil field (70 km to the NE). Within the subsidence belt, the Silayy Formation, especially the upper part, displays chaotic folding, including basin and dome structure expressed as a concordant hummocky topography attributable to differential interstratal dissolution and subsidence. Locally, inliers of E-dipping Yamamah Formation occur in the floor of the Ad Dilam depression, their position indicates a vertical subsidence that may exceed 120 m (Memesh et al., 2010). Outcrops of the Umm Sha'al formation, consisting of indurated alluvium and lacustrine limestone and gypsum occur in the Ad Dilam depression, partially filling the accommodation space created by dissolution subsidence. This formation, with an exposed thickness of around 30 m, locally shows dips of around 22°E that attenuate upwards (growth strata), recording deposition coeval to dissolution subsidence (i.e., synsedimentary subsidence).

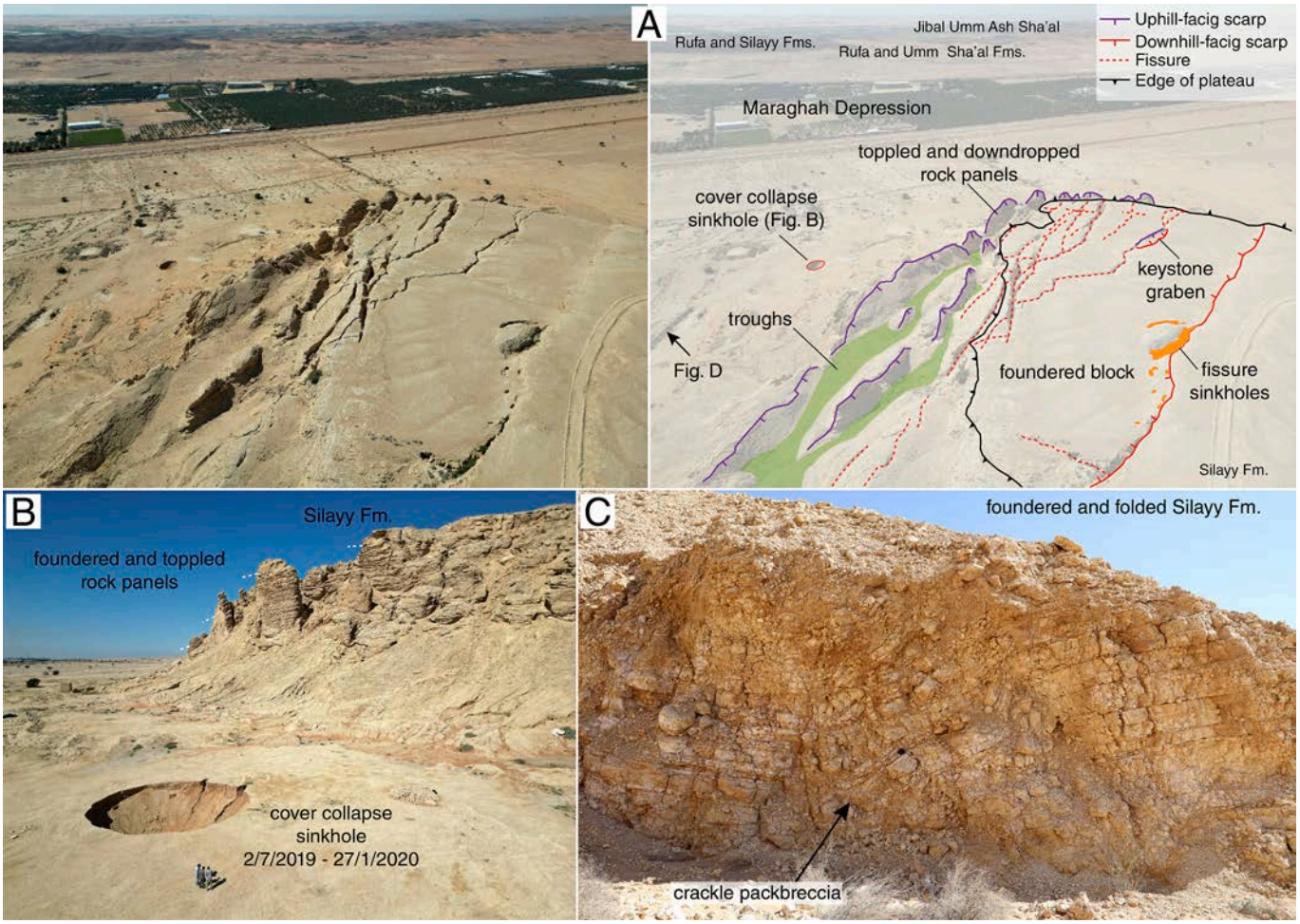

Fig. 15. Images of the Jabal al Jubayl escarpment at a salient with abundant fresh-looking extensional-collapse surface ruptures (38R 716486E 2,696,502 N). A: Downward view of the scarp showing evidence of active collapse and outward rotation of the Silayy limestone above the dissolution front, expressed as normal faults scarps, keystone grabens, fissures, toppled blocks and intervening troughs. B: Recent cover collapse sinkhole on alluvium at the foot of the scarp, formed between July 2019 and January 2020. D: Collapsed, folded and fractured Silayy limestone at the foot of the scarp, locally showing a crackle packbreccia (see location of outcrop in B). Buckle folding can be attributed to inner-arc contraction in the lower hinge of the monocline.

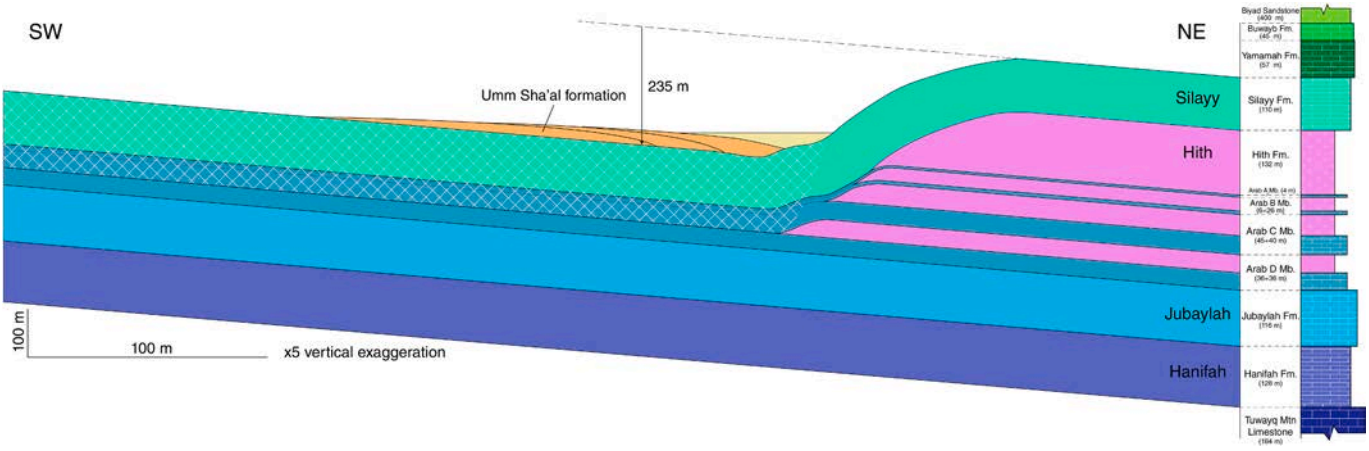

Fig. 16. Schematic cross-section across the Jabal al Jubayl monoclinal scarp and the associated subsidence trough partially filled by the Umm Sha'al formation (late Neogene-early Pleistocene?). The section considers a regional dip of 1°, the thickness of the Arab and Hith formations at the Abu Jifan oil field, and thicknesses reported by Vaslet et al. (1991) for the non-evaporitic formations in Ar Riyadh area. It assumes complete dissolution of anhydrite units lacking insoluble residues, and no bulking effect (volume increase) in the collapsed units, indicating a maximum vertical subsidence of 253 m. Note the general offlap arrangement of the sediments filling the NE- and downward-propagating subsidence trough.

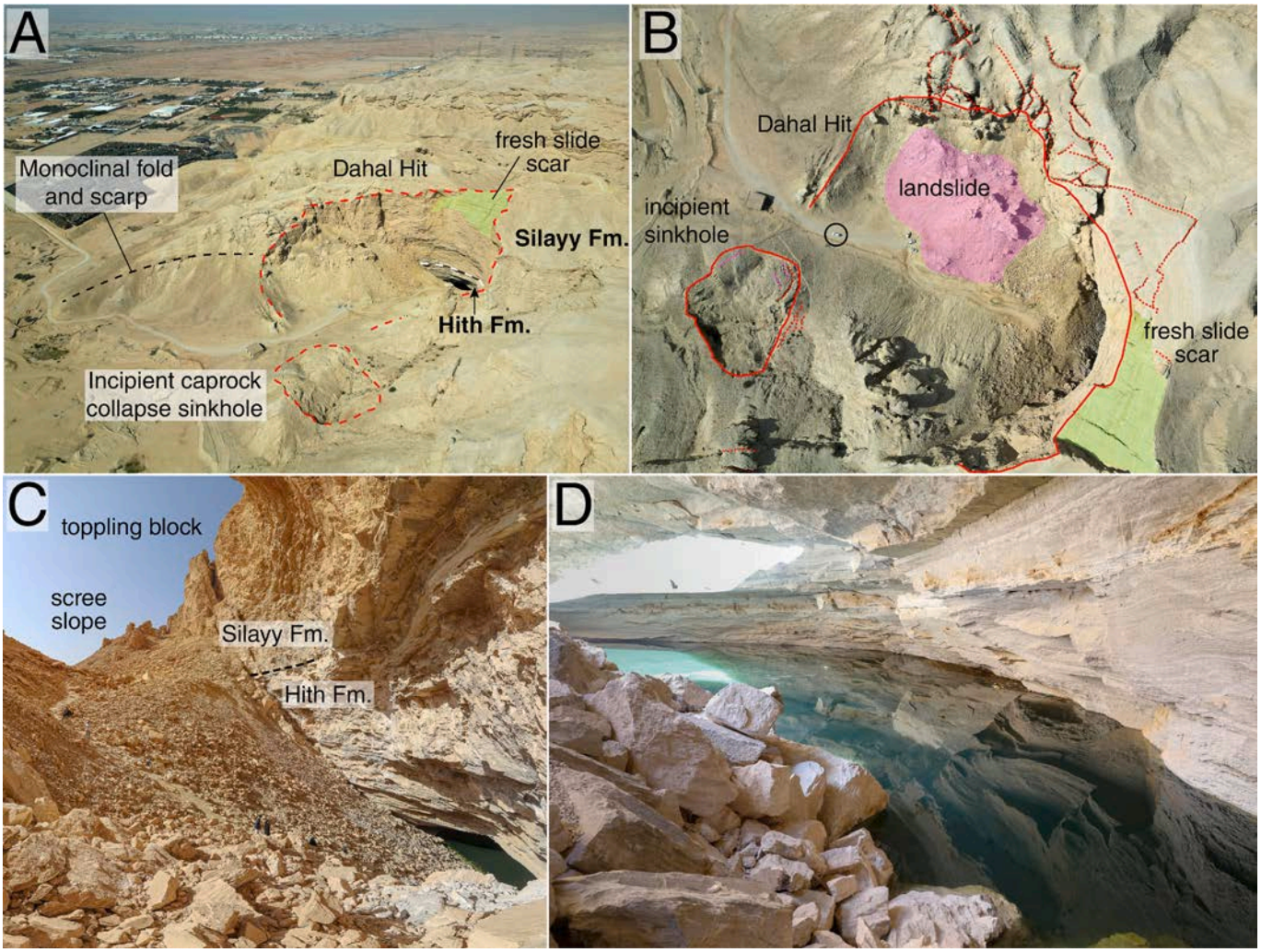

Fig. 17. Images of Dahl Hit sinkhole and cavern with an exposure of the Hith anhydrite (38R 702378E, 2,709,459 N). A, B: View of the monoclinal scarp punctured by Dahl Hit sinkhole and an adjacent incipient collapse sinkhole. Note expansion of the Dahl Hit sinkhole by rockfalls and rockslides. C: Dahl Hit, with a large scree slope at the entrance and a highly unstable overhanging wall on limestone and anhydrite in the inner part. D: Lake in the bottom of Dahl Hit, with high water level related to artificial recharge of the Silayy limestone aquifer from nearby artificial lakes filling old gravel pits.

The E-facing Jibal al Qusayah monoclinal scarp, up to 85 m high, has a discontinuous sinuous trace, with a large embayment 15.5 km long associated with a right-stepping step over. The aggregate cartographic and the straight lengths of the discontinuous scarp are 129 and 117.1 km, respectively, indicating a sinuosity index of 1.1. The southern termination of the scarp is associated with a NW-SE-oriented and down-to-the-SW monoclinal flexure oblique with respect to the general structural grain. Memesh et al. (2010) designated this structure as the Mihraqah Fault, and indicated that it could be a shallow gravitational structure related to interstratal evaporite dissolution with Quaternary activity. The Ad Dilam depression has extensive tracts of land with poorly integrated and disrupted drainage. The eastern trough of the depression at the foot of the scarp is drained by the NE-directed Wadi al Aqimi, which is interrupted in a depression with a 30 km long and NNE-SSW oriented succession of internally drained khabras. These enclosed basins and the large khabra located in the western trough of the Ad Dilam depression most probably represent the areas affected by greatest subsidence, functioning as terminal enclosed basins for the surface drainage. Currently, active gypsum deposition in these ephemeral lakes suggest the upward discharge of groundwater that has interacted with anhydrite of the Arab and Hith formations.

6. Morpho-structure of the monoclinal fold scarp

The monoclinal scarp developed over the dissolution front in the Hith Formation displays significant along-strike morpho-structural variability in the different sections. Deformation structures and surface ruptures on the upper anticlinal hinge (scarp crest) and in the middle limb (dipslope) are well exposed, while the lower synclinal hinge is largely concealed by Quaternary deposits. According to the geological maps the thickness of downthrown sediments overlying the Hith anhydrite varies between 100 and 300 m; (Ash Shib, 100–300 m; Ath Thumamah, 149 m; Jabal al Jubayl, 212 m; Jibal al Qusayah, 167 m). The observed surface deformation associated with the scarp reveals the subsidence mechanisms and allows the inference of the main controlling factors. The interstratal dissolution of the anhydrites through the downdip propagation of a dissolution front involves a progressive mass depletion beneath the overlying formations. Differential subsidence of sediments atop an updip sloping dissolution front is essentially achieved by both downward vertical displacement and outward rotation. The investigated monoclinal scarp illustrates that the localized gravitational deformation, restricted to the undermined supra-evaporite units, can be accommodated through various mechanisms that can be described by two end-member structural styles: (1) Brittle-dominated deformation with the downward rotation of rigid blocks on the sloping dissolution

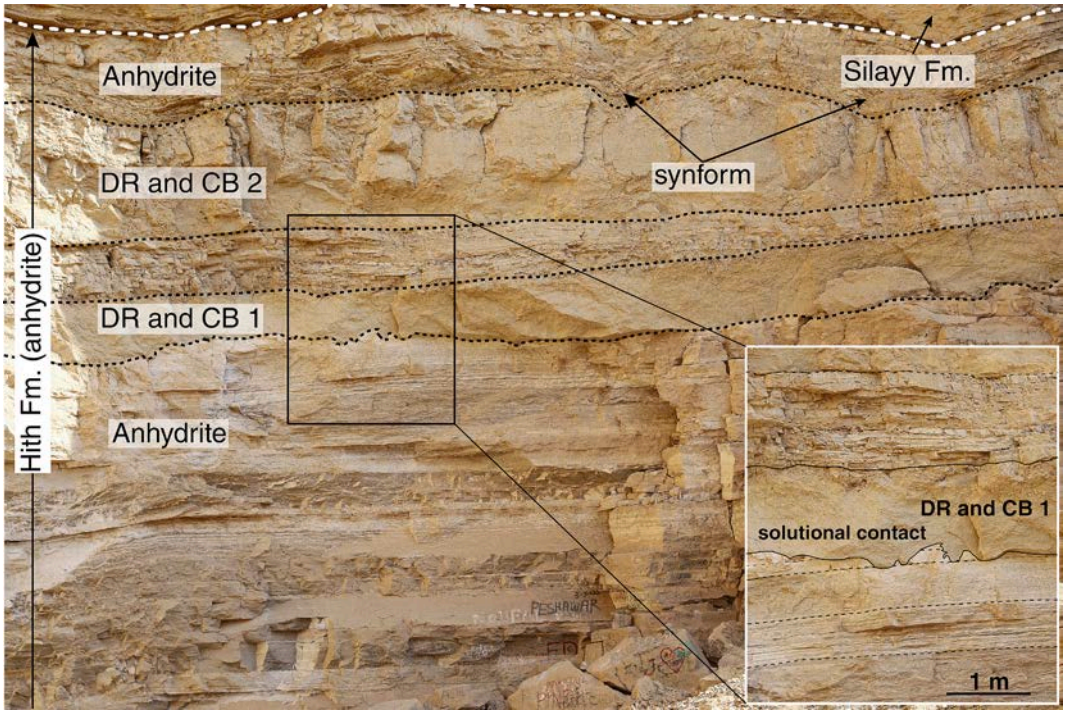

Fig. 18. Upper part of the Hith Formation exposed in Dahl Hit, showing two layers of dissolution residue and collapse breccias (DR and CB) interbedded within the anhydrite. The irregular base of these residual layers that truncate the underlying anhydrite beds is related to postsedimentary interstratal dissolution. The base of layer DR and CB1 was initially interpreted as a primary erosional unconformity or disconformity.

front and the development of upward-widening tension fissures and normal faults along their upper edge (i.e., articulated monocline; Powell, 1873, McCalpin, 2005) (Figs. 12C, 14A; 21A). (2) Ductile-dominated deformation through the development of a monocline draping the sloping dissolution front (passive bending) (Figs. 9C, 14B, 21B). Monoclinal folding involves the lengthening of strata, which can be accommodated by continuous deformation and/or the development of extensional structures (fissures, normal faults, keystone grabens). Additionally, outer-arc stretching also contributes to the development of extensional structures in the upper hinge of the monocline (fissures, crestal grabens) (Fig. 21C), while shortening structures may form in the lower hinge of the monocline affected by inner-arc contraction (e.g., buckle folds) (Figs. 15C, 21D). Irregularities in the sloping dissolution front can control the development of synthetic normal faults with significant throw, and antithetic normal faults, both expressed as downhill- and uphill-facing scarps, respectively (Figs. 9A, 12A, C, 21E). More complicated structures may develop associated with complex dissolution fronts involving various evaporite units, and where the removal of evaporite units by interstratal dissolution is incomplete.

In addition to the rheological properties of the rocks, two additional factors seem to play an important role in the morpho-structural style, namely the inclination of the dissolution front and the thickness of the deformed package. A steeper dissolution front determines the formation of monoclines with tighter hinges, favouring the development brittle extensional and contractional structures along the crest and lower hinge, respectively. Conversely, monoclinal folds on gently inclined dissolution fronts tend to display limited brittle deformation structures (Fig. 14B). The width of the upper hinge increases with the thickness of the bent sedimentary package, inhibiting the development of crestal extensional structures and favouring more distributed ruptures (Fig. 9C). In sinuous sections of the scarp, inner-arc contraction can occur at periclines associated with concave sections, resulting in the development of buckle detachment antiforms that may be expresses as scarp-normal ridges (Fig. 12A, B).

A peculiarity of these dissolution-induced monoclinal folds is that the position of the drape fold experiences progressive down-dip displacement in concert with that of the migrating dissolution front. The non-stationary nature of the gravitational deformation has two main long-term implications: (1) The stretched rocks of the upper hinge are transferred to the lower hinge of the monocline, where inner-arc contraction tends to close the extensional structures, involving a local change in stress regime. (2) The axis of the asymmetric depositional trough developed on the lower syncline experiences both lateral and downward displacement, in as much as dissolution affects evaporites situated at progressively lower elevation.

The surface ruptures (fault scarps, fissures) in some scarp sections show a fresh appearance, indicating active or recent interstratal dissolution and subsidence. The recency of these ruptures is revealed by fresh rock exposures lacking weathering patinas (Fig. 15A). Locally, these extensional structures disrupt drainages (e.g., blocked and beheaded streams, wind gaps) (Fig. 12C). Under the current climatic regime and considering the relatively low solubility of anhydrite/gypsum compared with salt, interstratal dissolution and subsidence are most probably very slow processes, but can be locally enhanced by favourable hydrogeological conditions related to natural and anthropogenic factors.

7. Sinkholes

A total of 107 caprock collapse sinkholes associated with the monoclinal scarp have been mapped (Figs. 7, 9, 11, 12, 14, 17). This value indicates an overall linear density of 0.27 sinkholes/km considering the cartographic length of the scarp (394 km). The highest density is found in the Ash Shib section (118 km long), with 71 sinkholes and a density of 0.6 sinkholes/km (Figs. 7, 9). The number and linear density of sinkholes in the 129-km-long Jibal al Qusayah section south of Ar Riyad drops to 23 and 0.17 sinkholes/km, respectively. The inventoried sinkholes comprise both enclosed (53) and open (54) depressions. The category of open sinkholes includes collapse depressions with external drainage that preserve more than half of its perimeter. In some sections the scarp is scalloped by amphitheatre-like concavities corresponding

Table 1
Chemical analyses of water samples collected at Dahl Hit in November 2019. Concentrations and total hardness in mg/L. Saturation indexes (SI) calculated considering a temperature of 25 °C and with the PHREEQC code and using the WATEQ4F database of thermodynamic data. $SiO_{2(am)}$ SI refers to the saturation index of amorphous silica. Analyses carried out by the Chemical and Physical Analysis Unit of the Saudi Geological Survey.

Sample	Ca	Mg	Na	K	Fe	Cl	HCO_3	NO_3	SO_4	F	NO_2	PO_4	SiO_2	eqCl/eqNa	$eqSO_4$/eqCa	TDS	Cond (us/cm)	pH	Total hardness	Gypsum SI	Anhydrite SI	Halite SI	Calcite SI	Dolomite SI	$SiO_{2(am)}$ SI
DA1	943.1	56.4	127.6	32.4	0.03	296.1	209	1.6	1950	1.0	1.6	<0.01	83.0	1.5	0.86	3610.8	4580	7.0	2587.1	0.14	−0.080	−6.120	0.407	−0.08	−0.139
DA2	940.0	49.7	123.0	35.4	0.08	292.7	197	0.7	1946	1.0	0.7	<0.01	69.2	1.54	0.86	3554.8	4560	6.8	2551.5	0.14	−0.088	−6.141	0.192	−0.558	−0.218

old open and degraded sinkholes (Figs. 9, 11). The transformation of the caprock collapse sinkholes from closed to open is mainly related to: (1) subsidence and outward rotation in the monoclinal scarp related to interstratal dissolution; (2) erosion at the sinkhole margins, mostly by mass wasting processes leading to the flattening of the margins and aggradation in the floor (i.e., expansion and shallowing of the depression); and (3) capture by headward propagating gullies. The two former processes tend to transform cylindrical shaft-like sinkholes into conical or tronco-conical depressions, and eventually into amphitheatre-like basins opened on the downslope side and enclosed by an arcuate backscarp on the upslope side, resembling heelsteps (Figs. 9, 11).

Two morpho-chronological sinkhole types with distinctive morphometric parameters have been differentiated (Table 2): (1) immature cylindrical sinkholes (31 sinkholes; 29 %) with subvertical to overhanging sides (Fig. 12B, 14A); and (2) mature conical (or tronco-conical) sinkholes (76 sinkholes; 71 %) with sloping bedrock slopes resulting from long-sustained erosional degradation and expansion of former shaft-like sinkholes (Figs. 9, 11C). A great proportion of the sinkholes, including both cylindrical and conical, show evidence of active mass wasting such as detached and toppling blocks and recent rockfall deposits (Fig. 17). Cylindrical sinkholes show contrasting relative frequencies north of Ar Riyadh (13 out of 84; 15.5 %) and south of Ar Riyadh (16 out of 23; 65.6 %). A total of 9 sinkholes (8.4 %) correspond to compound depressions, which may be related to the coalescence of two adjoining sinkholes (e.g., slope degradation, fluvial erosion) (Fig. 11C), or the intersection of a pre-existing sinkhole by a more recent collapse.

Regarding the distribution of sinkholes within the monoclinal-fold scarp, 13 % occur in the crestal zone or upper hinge (14 sinkholes), 63 % in the slope or middle limb (67 sinkholes), and 24 % at the foot (26 sinkholes), with part of the sinkhole edge at the elevation of the piedmont (e.g., Figs. 9C, 11D). The relative proportion of the more recent, fresh-looking cylindrical sinkholes is higher in the slope and foot sections of the scarp; crest (21.4 %), slope (31.3 %), foot (27.7 %). Closed sinkholes exhibit lower relative frequency at the foot (31 %) than at the slope and crest (both 57 %). Some sinkholes occur spatially associated with fold-parallel fissures and fault scarps. In some cases, it is possible to ascertain that the sinkhole is offset by a fault (e.g., faulted floor underlain by sinkhole deposits), indicating that the fault has been active after the formation of the collapse sinkhole (Fig. 11A). In other cases, the relative chronology remains ambiguous. For instance, the presence of fault scarps at the margins of a sinkhole could be related to the occurrence of a collapse on an already faulted surface, and/or fault displacement after sinkhole occurrence.

The single sinkholes have a dominant subcircular geometry, as indicated by a mean circularity ratio of 0.91. The circularity ratio is computed dividing the area of the sinkhole by the area of a circle having a circumference equal to the perimeter of the sinkhole, thus the closer the value to 1, the closer it is to a perfectly circular geometry in plan. The mean circularity ratio drops to 0.56 for the cylindrical sinkholes, which often display polygonal and irregular geometries controlled by the fracture pattern, evolving into more circular geometries as the scarped edges degrade by mass wasting (Fig. 11B). All sinkholes (single and compound), single sinkholes, and cylindrical single sinkholes show low mean elongation ratios (length/width) of around 1.3. The length and width of the sinkholes have been extracted automatically using the Minimum Bounding Geometry tool and the Convex Hull Option of ArcGISpro. Both the low elongation and the high circularity are consistent with the high dispersion of the orientation of the major axes of the sinkholes.

A remarkable feature of the caprock collapse sinkholes is their large planimetric dimensions, attributable to both the high mechanical resistance of the caprock above a deep-seated karst and the expansion of depressions by erosion at their margins (De Waele and Gutiérrez, 2022). The main statistics for all the sinkholes, the single sinkholes and the single cylindrical sinkholes are presented in Table 2. The sinkhole with

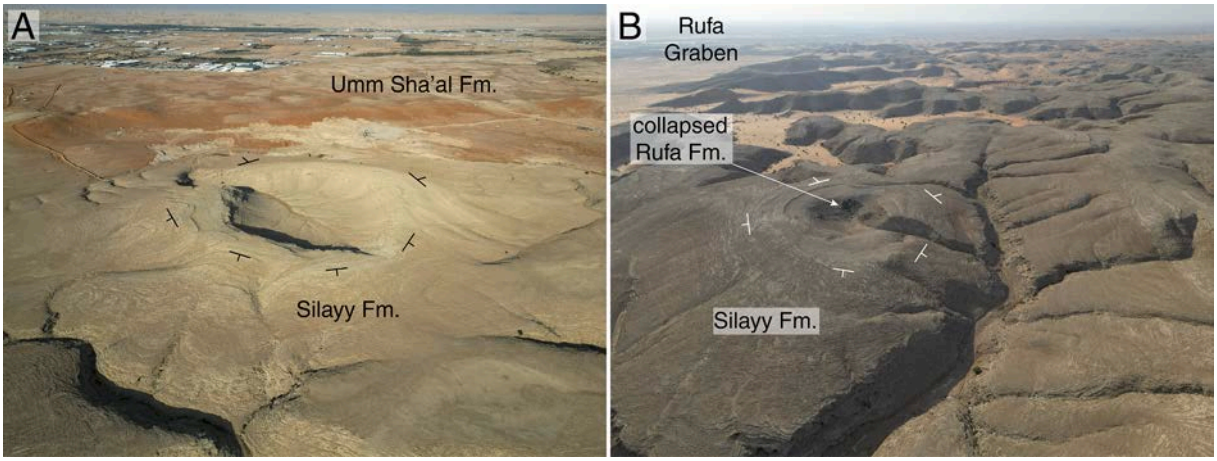

Fig. 19. Outcrops of the Silayy Formation showing a complex basin and dome structure. A: Hill on dome structure with an inner crater-like depression with external drainage. Outcrops of Umm Sha'al formation dipping towards the dissolution-induced basin in the background. B: Dome structure in the northern margin of the Rufa Graben with an inner depression hosting remnants of foundered Rufa formation.

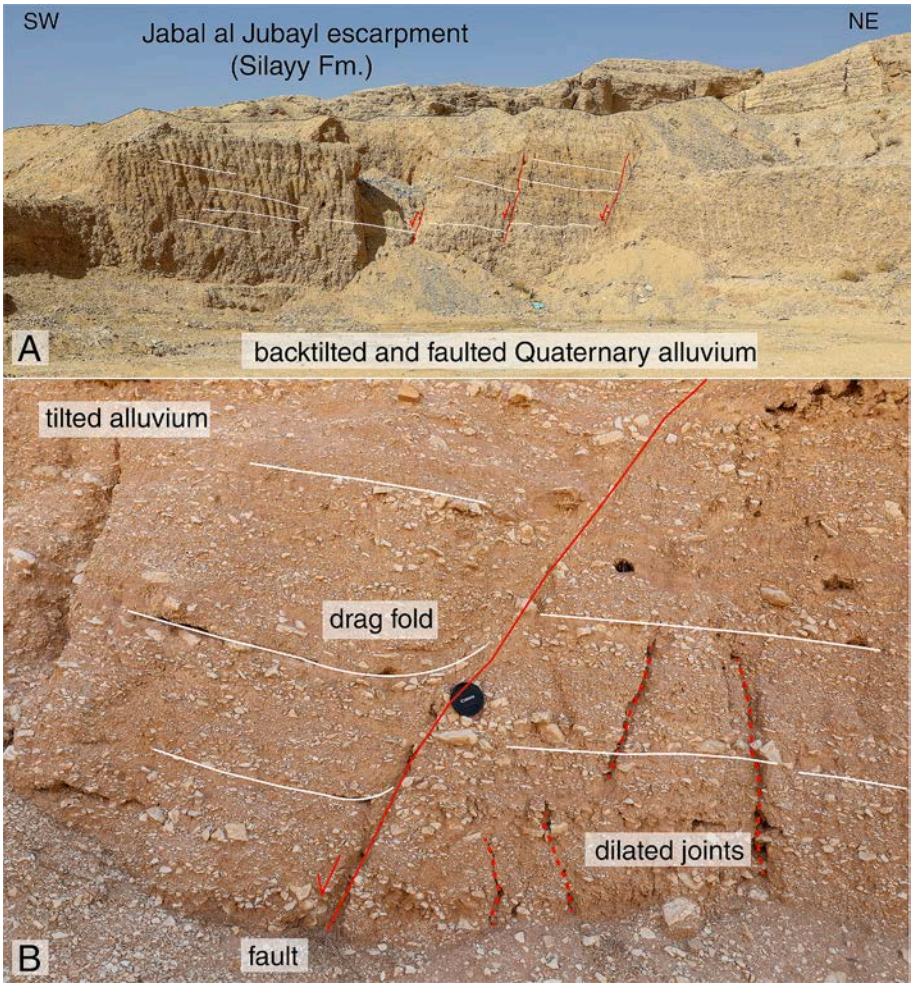

Fig. 20. Deformed Quaternary alluvium at the foot of the Jabal al Jubayl escarpment south of Dahl Hit recording recent dissolution-induced subsidence (38R 702475E 2,709,191 N). White lines stand for bedding and red lines for faults and fractures. A: Backtilted and faulted alluvium. B: Close-up view of tilted alluvium with normal faults and dilated joints. Lens cap 8 cm in diameter for scale. (For interpretation of the references to colour in this figure legend, the reader is referred to the web version of this article.)

the largest length (619 m) is a compound depression resulting for the coalescence of two sinkholes (Fig. 11C). The maximum and mean length of the 98 single sinkholes, including both conical and cylindrical, are 413 m and 117 m, respectively. These parameters drop to lower values when considering only the 29 shaft-like single sinkholes; 178 m maximum length and 65 m average length. This morphometric deviation

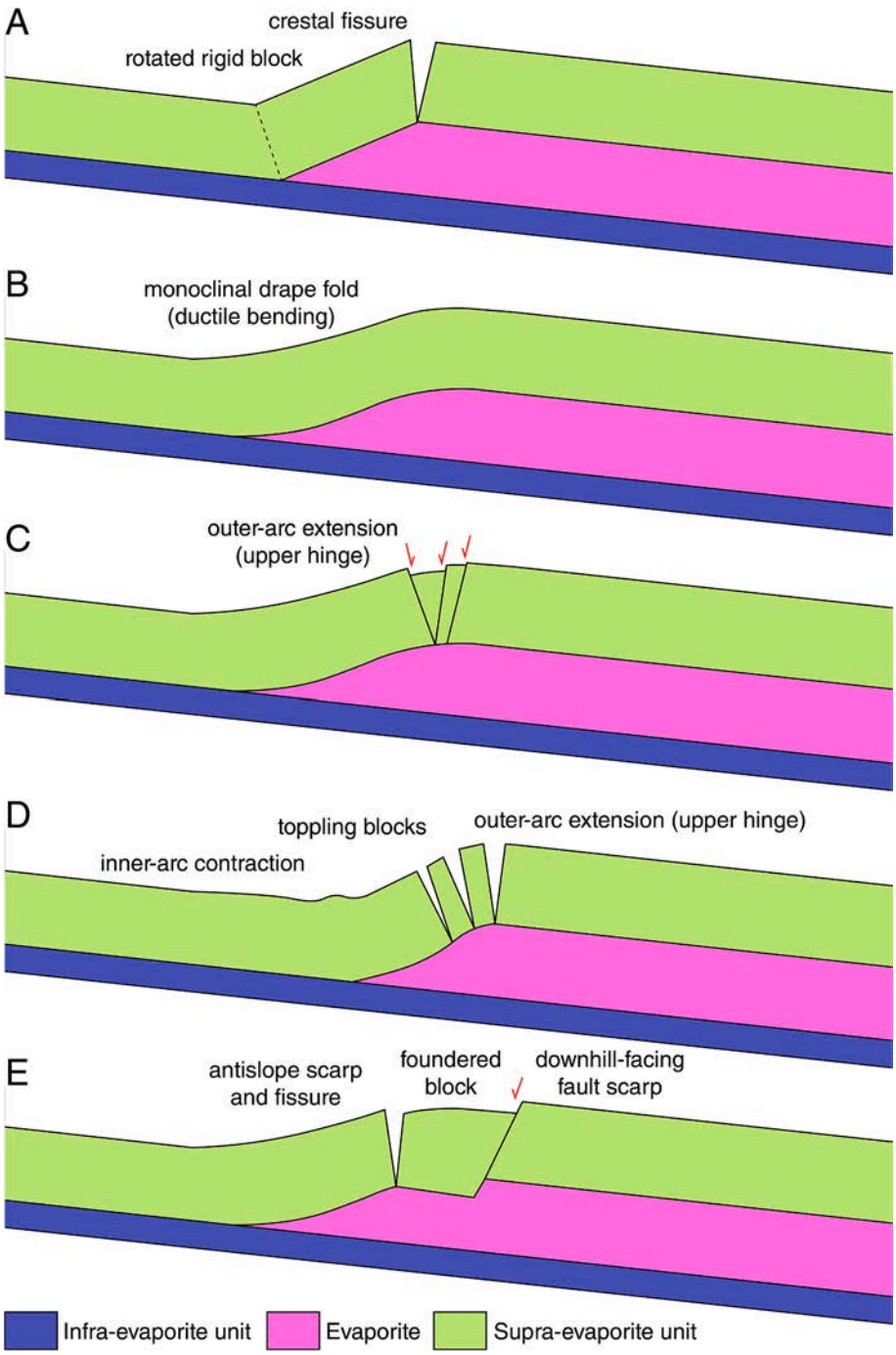

Fig. 21. Schematic cross-sections showing different morpho-structural styles in monoclinal fold scarps associated with down-dip migrating dissolution fronts. See text for explanation.

reflects the long-term areal growth of the collapse sinkholes through the degradation and recession of the slopes (e.g., Gökkaya et al., 2021).

The graph in Fig. 22 plots sinkhole lengths (major axis) of single sinkholes (98) and cylindrical single sinkholes (29) in a logarithmic scale versus cumulative frequency of sinkholes equal or larger than a given length in the analysed monoclinal scarp. The figure also shows data from various evaporite karst environments (gypsum and salt; covered, bare and interstratal; epigene and hypogene): (1) single cover collapse and sagging sinkholes in the mantled eogenic salt karst of the Dead Sea, where depressions experience significant expansion by mass wasting acting on their margins (Sevil and Gutiérrez, 2023); (2) single bedrock collapse sinkholes in the Sivas gypsum karst (Turkey) that reach exceptionally large dimensions due to post-collapse enlargement by erosion (Gökkaya et al., 2021); (3) mainly caprock collapse sinkholes in the deep-seated hypogene interstratal gypsum karst of the Sant Miquel valley, NE Spain (Gutiérrez et al., 2019); (4) collapse sinkholes in the Anbal salt pillow with a gypsum-rich caprock (Gutiérrez and Lizaga, 2016). The length of all the single sinkholes mapped in the monoclinal scarp covers covers 1.8 orders of magnitude (413 to 6 m) and follows a power-law distribution for a significant part of the size spectrum, with a well-defined roll-over for the smaller sinkholes. The length of the cylindrical single sinkholes displays significantly lower values (178 to 65 m), a much more restricted range (0.4 orders of magnitude), and a power-law distribution for most of the size range. These differences

Table 2
Main statistics for different groups of caprock collapse sinkholes inventoried in the monoclinal scarp; all sinkholes, single sinkholes and single immature sinkholes with cylindrical geometry.

		Perimeter (m)	Area (m^2)	Length (m)	Elongation	Circularity
Caprock collapse (all, 107)	Mean	361.73	13,191.69	125.92	1.30	0.90
	Median	347.85	9032.16	118.84	1.21	0.94
	Std. dev.	240.60	21,521.51	84.91	0.24	0.09
	Max.	1728.16	191,484.05	619.44	2.42	0.98
	Min.	16.59	20.79	5.95	1.05	0.56
Caprock collapse (single, 98)	Mean	338.86	10,987.56	117.44	1.28	0.91
	Median	345.43	9025.16	117.62	1.21	0.94
	Std. dev.	192.31	12,323.91	66.36	0.22	0.08
	Max.	1126.86	91,086.62	413.08	2.42	0.98
	Min.	16.59	20.79	5.95	1.05	0.86
Caprock collapse (single cylindrical, 29)	Mean	185.48	3334.33	65.35	1.35	0.56
	Median	185.31	1876.88	66.37	1.30	0.90
	Std. dev.	127.73	4458.93	43.73	0.24	0.11
	Max.	524.36	20,655.44	177.86	2.42	0.96
	Min.	16.59	20.79	5.95	1.13	0.56

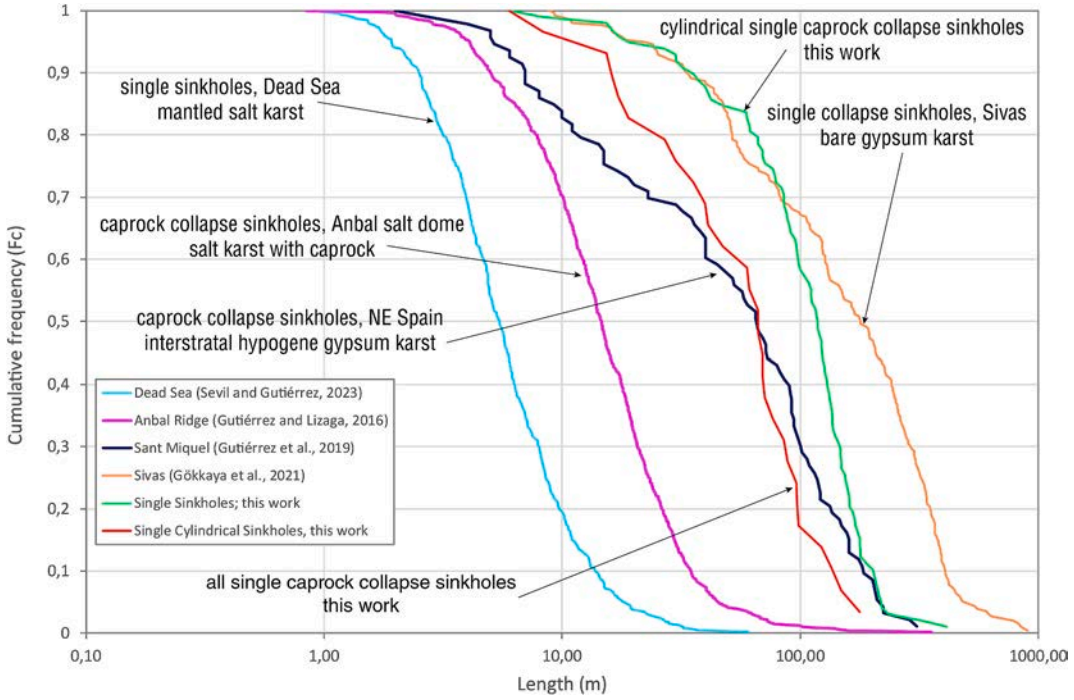

Fig. 22. Graphs of sinkhole length (major axis) versus cumulative frequency (frequency of sinkholes equal or larger than a given length) in the monoclinal scarp (single sinkholes and single cylindrical sinkholes), as well as in various types of evaporite karst environments (gypsum and salt; covered, bare, and interstratal; epigene and hypogene).

reflect the fact that the population of all single sinkholes include a wider chronological and morphogenetic spectrum of sinkholes, from inmature ones essentially related to the collapse of cavity roofs, to old and relatively larger sinkholes resulting from both initial collapse and protracted periods of expansion by the erosional recesion of the margins. The size of the single cylindrical caprock collapse sinkholes in the monocline is comparable with that of the caprock collapse sinkholes of the hypogene gypsum karst of Sant Miquel in NE Spain, both occur in an interstratal karst. The single caprock collapse sinkholes, including both conical (mature) and cylindical (inmature), show smaller sizes than the single bedrock collapse sinkholes of the Sivas gypsum karst, where bedrock has higher erodibility than the limestone caprocks of our study area, and thus sinkholes expand much more rapidly (Gökkaya et al., 2021).

8. Associated hazards

The number of reported historical sinkholes is relatively small compared with the dimension of the subsidence belt and monoclinal fold scarp associated with the dissolution front of the Late Jurassic anhydrites. However, the historical sinkholes show a clear spatial and temporal association with anthropogenic activities, locally reaching high densities and probabilities of occurrence. A large collapse sinkhole has been documented in the Ath Thumamah Depression at the projection of the monoclinal fold scarp atop the dissolution front (38R 679611E 2,782,485 N; Ath Thumamah section in Fig. 7; Fig. 13). Historical imagery indicates that this rapidly growing sinkhole formed sometime between December 2017 and July 2019, and that its length increased from 22 m to 50 m (expansion rate of 15.5. m/yr). In a field visit on January 2023 the sinkhole displayed an elliptical planform 55 m long and 37 m wide, and a depth of 27 m. These dimensions indicate a volume of around 40,000 m^3, providing a minimum estimate for the size of the subsurface cavity responsible for the collapse. This volume strongly indicates that it corresponds to a caprock and cover collapse sinkhole, likely related to dissolution of the Hith anhydrite and the development

of a transtratal breccia pipe by progressive upward collapse (i.e., stoping). This sinkhole, associated with a buried water pipe, was probably induced by water leakage.

At the Al Nadwa suburb of Ar Riyadh, where the city has expanded across the monoclinal fold scarp atop the dissolution front, the occurrence of a collapse sinkhole was reported at the foot of the scarp, leading to the abandonment of a plot of land (38R 691810E 2,746,042 N; Fig. 23). Historical satellite imagery indicates that the sinkhole occurred between November 2004 and April 2008 and that it has experienced post-May 2009 reactivation after its artificial fill.

A dense cluster of at least 20 historical collapse sinkholes occur associated with artificial lakes located 10 km SE of Dahl Hit (Figs. 6, 24). Here, treated sewage water is poured into large gravel pits located at the foot of the monoclinal fold scarp overlying the dissolution front. The lakes host collapse sinkholes that function as ponors (swallow holes), one of them showing massive water losses and aquifer recharge via a water fall (Fig. 25), consistent with the rapid water table rise documented since the creation of the lakes (Michelsen et al., 2019). Most of the sinkholes occur on unconsolidated deposits at the foot of the scarp and to the *E*-NE of the lakes, suggesting preferential groundwater flow and evaporite dissolution in that direction. The bracketed ages of the cover collapse sinkholes established with historical imagery indicates that all of the them are younger than the infill of the lakes that started sometime between 2009 and 2011 (Fig. 24). An additional cover collapse sinkhole occurred at the foot of the scarp between July 2019 and January 2020, around 7 km to the SE of the lakes, it has probably also been induced by artificial groundwater recharge (Fig. 15A, B). At 2.7 km SE of Dahl Hit, a collapse sinkhole that occurred between May and October 2020 caused the sudden destruction of a building (38R 703342E 2,706,868 N; Fig. 26) (Al-Hashim et al., 2024). This case illustrates the potential threat posed in the foreseeable future by new sinkholes on man-made structures and people.

9. Discussion

Subsidence morpho-structures related to the downdip propagation of dissolution fronts in gently dipping evaporite formations occur in a number of regions worldwide. This long-term and large-scale interstratal dissolution and subsidence phenomenon generates supra-evaporite monoclinal folds atop the dissolution front and structural troughs along the evaporite-depleted belt. The documented cases occur in large and slightly deformed (i.e., gently tilted) Phanerozoic evaporite basins that have been the subject of intense geological investigations, partly for oil and salt exploration (e.g., North America, Saudi Arabia, United Kingdom). These circumstances suggest that this type of dissolutional edge overlain by gravitationally deformed strata may be present in other less investigated evaporite basins, but have so far gone unnoticed. A great proportion of these dissolution and subsidence features are associated with salt units, but they also occur in much less soluble gypsum/anhydrite units (Roswell Artesian Basin in New Mexico,

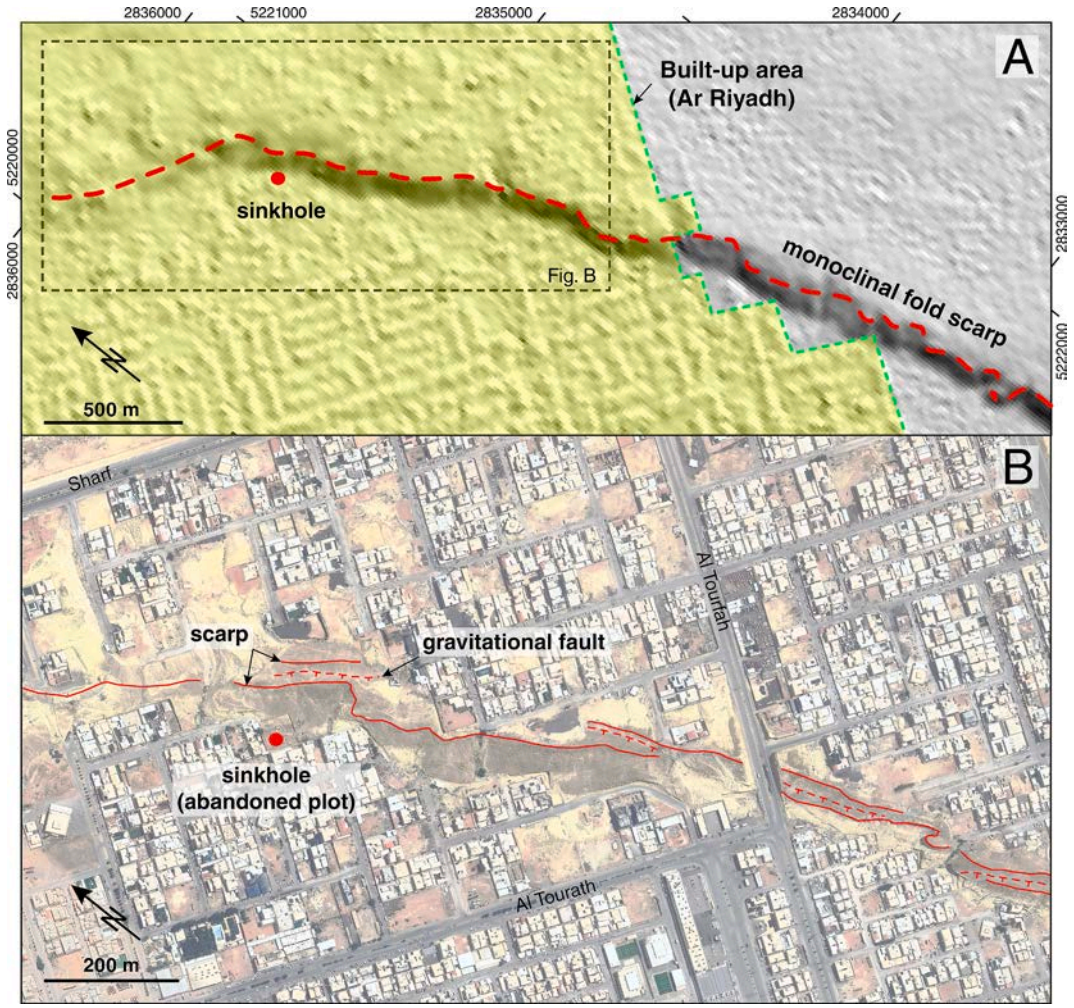

Fig. 23. Hillshade and satellite image illustrating the expansion of Ar Riyadh city across the unstable ground associated with the monoclinal fold scarp. The scarp locally shows a compound profile related to the presence of gravitational collapse faults. A sinkhole occurred between 2004 and 2008 at the foot of the scarp, leading to the abandonment of a plot of land (38R 691810E 2,746,042 N). Satellite image (April 2023) captured from Google Earth.

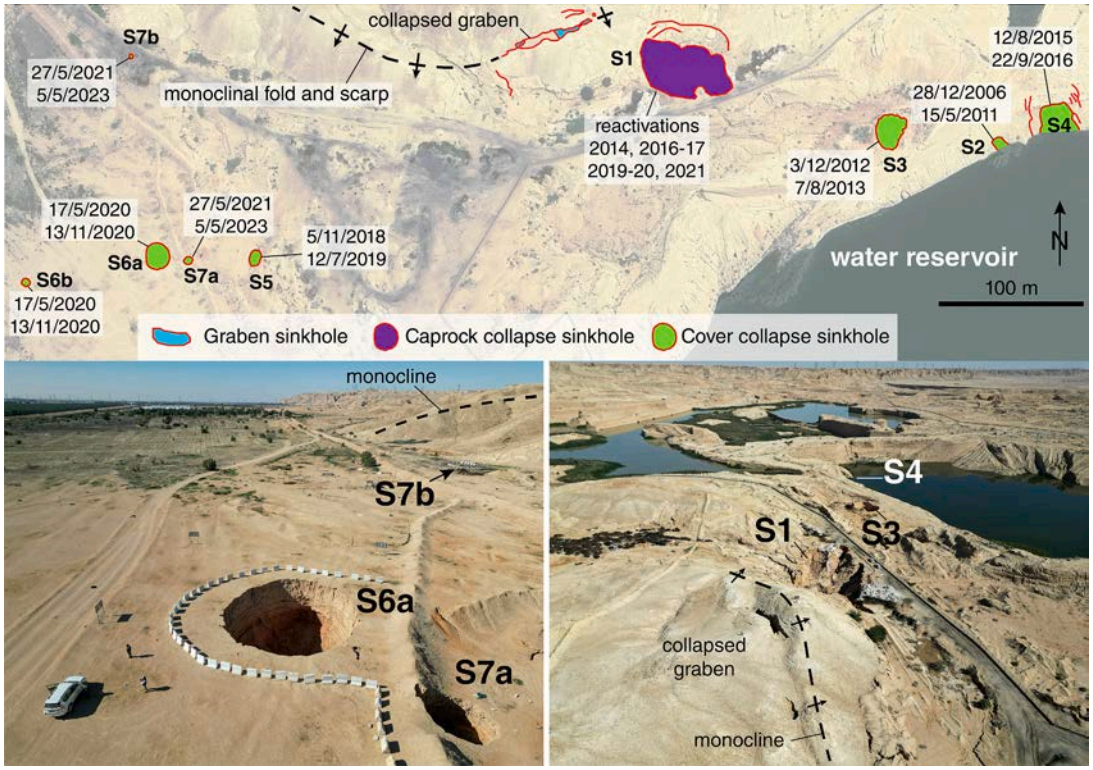

Fig. 24. Historical collapse sinkholes spatially and temporarily associated with artificial lakes filling gravel pits next to and above the dissolution front of the Hith anhydrite. The timing of sinkhole occurrence or reactivation has been determined using historical imagery from Google Earth.

Permian gypsum NE England, central Saudi Arabia). These subsidence morpho-structures, commonly expressed in the landscape by a monoclinal scarp and an adjoining depression, constitute the largest karst features of our planet (De Waele and Gutiérrez, 2022). The biggest salt karst feature is the ca. 1000 km long subsidence belt associated with the Middle Devonian Prairie Salt in western Canada (Broughton, 2017, 2021). The largest Ca-sulphate karst feature worldwide is the dissolution and subsidence belt developed along the updip edge of the Upper Jurassic Hith and Arab anhydrites in the Interior Homocline of Saudi Arabia. This dissolution-induced subsidence belt has a minimum length of 800 km and extends for an unknown distance to the south beneath the sands of the Rub' al Khali Erg (Fig. 6). Moreover, the example in arid central Saudi Arabia is the one where the associated structural, stratigraphic and geomorphic features are best displayed. Interestingly, Ar Riyadh, with around 8 million inhabitants, lies on this interstratal dissolution belt and the associated subsidence structures (Fig. 7).

The subsurface dissolution fronts that cut across the evaporite beds, often designated as salt slopes or salt scarps, typically have an updip-facing sloping geometry. Differential subsidence and rotation of the strata overlying these downdip propagating dissolution fronts is accommodated through the development of updip-facing monoclines (passive bending). These supra-evaporite folds show sharp local dip reversals in the middle limb draping the sloping dissolution front. The monoclines can be expressed in the landscape as long and prominent fold escarpments more than 100 m high. The largest and best displayed examples worldwide are the ones documented in this work, with sections ranging from 30 to 129 km long, and collectively forming a mega-landform with an aggregate length of 420 km (Fig. 7). The fold scarps may display a sinuous cartographic trace, with sharp embayments and pointed salients that reflect the differential lateral propagation of the dissolution front. In the dissolution-induced fold scarps of the Interior Homocline, the sinuosity index varies from 1.27 to 1.1, with the highest value in the 118 km long Ash Shib scarp (Fig. 7). The monoclinal folds may lack geomorphic expression in areas where surface deformation is overwhelmed by aggradation or erosion. The discontinuous character of the investigated fold scarp is mainly related to buried sections in areas with high sediment supply from nearby rapidly retreating erosional scarps (e.g., friable sands capped by limestone).

The monoclinal folds typically display extensional and collapse structures along the upper hinge (fissures, grabens, normal faults) related to bending-related layer lengthening and outer-arc extension, plus differential dissolution and subsidence (Fig. 21). The lower hinge of the monocline, although generally concealed by recent deposits, may show buckle folds expressed as longitudinal wrinkle ridges related to inner-arc contraction (Fig. 21D). These detachment antiforms can also develop in periclinal hinges associated with sharp changes in the fold trend (Fig. 12B). The mobile nature of these drape folds determines that, as the dissolution front migrates laterally, the layers stretched in the upper hinge move to the lower hinge, where inherited extensional structures then experience shortening. Some of the main factors that control the deformation style (brittle- versus ductile-dominated) and size of the monoclinal folds, in addition to the mechanical properties of the rocks, include: (1) The thickness of the evaporite unit and the proportion of insoluble material, which constrains the maximum structural relief of the monocline. In the Ar Riyadh area, the dissolution of the Arab and Hith anhydrites, with an aggregate thickness of around 235 m, has generated a monocline with an estimated throw of 150–200 m. (2) The inclination of the dissolution front, which determines the width of the monocline, the dip of the middle limb, and the curvature of the hinges, with influence on the development of bending-moment secondary structures. (3) The thickness of the folded supra-evaporite package, which influences the width of the hinges and the distribution of secondary bending-moment extensional and shortening structures. The fold scarps developed over the dissolution fronts are often punctured by large caprock collapse sinkholes, providing evidence of focused dissolution and formation of large cavities within the evaporites. The development and lateral migration of the dissolution-induced monoclinal folds can cause disruption in the drainage network. A common situation is the

Fig. 25. Collapse in the artificial lake area functioning as a swallow hole with massive water infiltration. The white colour corresponds to turbulence-generated foam from the treated sewage water.

progressive beheading of downdip transverse (consequent) drainages, in which upper channel sections experience progressive subsidence and gradient reversals. Excellent examples occur in the Holbrook Anticline, Arizona (Fig. 2) and in the Ash Shib scarp section (38R 596796E 2,860,817 N).

Differentiating between dissolution-induced monoclines and non-gravitational tectonic monoclines may have important practical implications. Dissolution-induced subsidence can create structural traps for oil or gas in bent strata atop dissolution fronts (i.e., evaporite-collapse anticlines; Oldham, 1996; Warren, 2016). Parker (1967) documents several cases associated with dissolved Middle Devonian and Permian salts in Wyoming and Montana. Moreover, abrupt thickness changes associated with dissolution fronts can create false images of the subsalt strata in seismic profiles, including phantom folds and faults (Oldham, 1996; Johnson and Timson, 2023). Non-existing infra-evaporite antiforms (phantom anticlines) or supra-evaporite structural highs may lead to false expectations in oil exploration. For instance, Lindsay et al. (2006) reported that wildcat wells were drilled along surface structural highs in Saudi Arabia (e.g., Ma'agala and El Alat), that happened to be shallow gravitational structures related to differential interstratal dissolution of lower Eocene Rus evaporite beds. This distinction may also have important implications for salt mining, nuclear waste disposal or seismic hazard assessment (e.g., monoclines underlain by active faults). The main criteria that can be used to identify dissolution-induced monoclines include: (1) deformation restricted to the supra-evaporite units; (2) structural relief not greater than the thickness of the evaporites; (3) dissolutional thinning of the evaporites, grading into dissolution residues and breccias within condensed stratigraphic successions; (4) fold axes with high sinuosity, including sharp embayments

Fig. 26. Collapse sinkhole that occurred in May–October 2020 around 2.7 km southeast of Dahl Hit, resulting in the destruction of a building (38R 703342E 2,706,868 N). New sinkholes can be expected in this areas subject to massive water infiltration from artificial lakes. Images captured from Google Earth.

and salients; (5) abundant and conspicuous extensional and collapse features with significant vertical displacement along the crest; and (6) presence of large caprock collapse sinkholes.

Caprock collapse sinkholes reach extraordinary large dimensions and high densities in dissolution-induced monoclinal scarps (Figs. 2, 5, 9, 11). The giant sinkholes found in these interstratal evaporite karst settings have been largely unappreciated. See for example the worldwide review on collapse sinkholes larger than 100 m across by Waltham (2005). Two morpho-chronological groups have been differentiated among the single sinkholes mapped in the analysed monoclinal scarps, namely immature cylindrical sinkholes (31, 29 %, up to 178 m long) and conical sinkholes with degraded margins (76, 71 %, up to 413 m long) (Table 2). The much larger size of the latter indicates significant post-collapse expansion by mass wasting process and slope recession. The highest sinkhole density is found in the Ash Shib section (118 km long), with 71 inventoried sinkholes and a density of 0.6 sinkholes/km (Fig. 7). The mapped sinkholes display an overall chronosequence across the

monoclinal scarp, showing a general more degraded appearance and older age towards the piedmont, consistent with the lateral migration of the dissolution front and fold scarp (Fig. 9C).

Subsidence associated with laterally migrating dissolution fronts generates asymmetric synformal troughs with a steep mobile margin defined by a monocline. These troughs may function as depositional basins during protracted periods of time, and may experience different phases of dissolution-induced subsidence and sedimentation. The timing of subsidence periods can be constrained by the sedimentary deposits filling the basins (Johnson, 1989), often displaying growth stratal geometries (i.e., progressive unconformities), or by formations showing thickening spatially associated with the dissolution troughs (e.g., Parker, 1967). In western Canada, the Early Cretaceous Athabasca Oil Sands where partially deposited in active dissolution-induced basins, showing evidence of synsedimentary sinkholes and subsidence (Broughton, 2013, 2015). In most cases, information on the age of the sediments that record dissolution-induced subsidence (i.e., synsedimentary subsidence) is poor, hindering the possibility of reconstructing the dissolution and subsidence history, and calculating long-term subsidence rates and lateral migration rates for the dissolution front. In central Saudi Arabia, the main dissolution phase seems to be constrained by the alluvial and lacustrine deposits of the Umm Sha'al formation, that reaches around 140 m thick in the Ar Riyadh area. However, the late Neogene-early Pleistocene age proposed for this formation remains rather speculative (Vaslet et al., 1991). The downdip propagation of dissolution fronts implies the long-term lateral and downward displacement of the subsidence troughs. The spatial-temporal pattern leads to sedimentary fills with an overall offlap arrangement, recording progressively younger deposition towards the monocline and at lower elevations (Fig. 27A).

As the dissolution front migrates, the dissolutional removal of the evaporite unit may not be complete. Evaporite residuals may remain behind the downdip propagating dissolution front, which may be expressed as structural highs with geomorphic expression (Fig. 27B). These evaporite remnants can be expressed as antiformal ridges (e.g., structural high within the Ad Dilam depression) or striking basin and dome morpho-structures related to differential dissolution and subsidence (Figs. 10, 19). The presence of enclosed crater-like depressions in the crest of domal hills, with nested foundered sediments once situated at higher elevations, suggest that they correspond to collapse structures related to the late dissolutional removal of evaporite residuals (Fig. 19B).

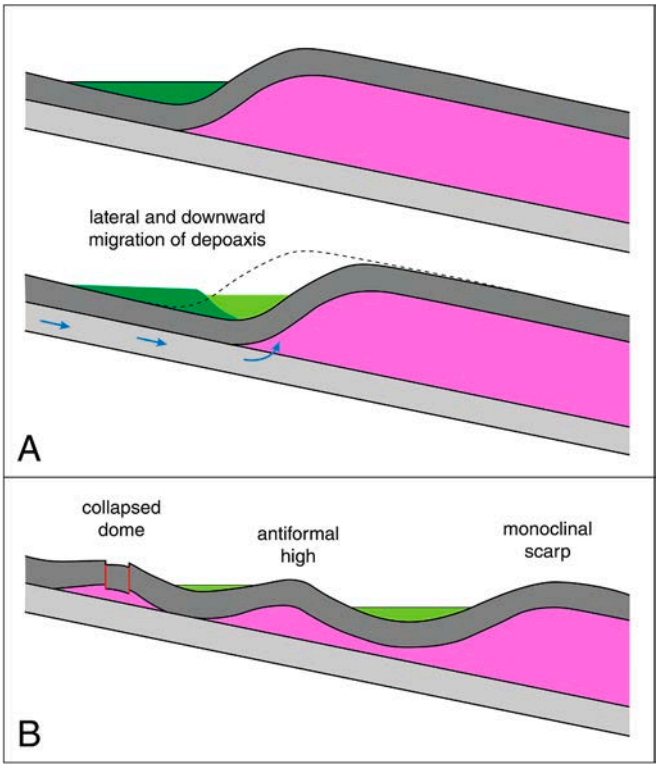

Fig. 27. A: Schematic cross-sections showing the lateral and downward displacement of depositional troughs associated with down-dip migrating dissolutional fronts, resulting in a sedimentary fill with an overall offlap arrangement. B: Cross-section illustrating morpho-structures associated with residual evaporites left behind the main dissolution front. Note dissolution-induced trough with an intra-basin high.

The subsidence troughs associated with downdip migrating dissolution fronts may reach hundreds of kilometres in length and may control the hydrographic network in different ways: (1) guiding the path and lateral migration of fluvial systems; (2) blocking longitudinal drainages at active subsidence basins; and (3) creating lakes in subsidence basins. In semiarid areas such as in central Saudi Arabia, playa-lakes in subsidence basins can be sites of evaporite deposition, representing the recycling of the evaporites removed by interstratal dissolution (Umm Sha'al formation, playa-lakes in the Ad Dilam depression; Vaslet et al., 1991; Memesh et al., 2010).

Two main hydrogeological models have been proposed to explain the development and migration of dissolution fronts; epigene and hypogene karst. In the epigene karst model, dissolution is mainly achieved by downward groundwater flow from an overlying or adjacent recharge area. Hypogene dissolution is caused by groundwater derived from an underlying aquifer. The Roswell Artesian basin in New Mexico is a paradigmatic example of hypogene dissolution (Land, 2003; Stafford et al., 2008). Epigene dissolution seems to be the dominant process in the Holbrook Anticline, Arizona, where dissolution seems to behave as a self-sustaining process by increasing the permeability in the overlying collapse sediments and enhancing water infiltration (Neal et al., 2013). This mechanism can be effective as long as there is groundwater circulation and renewal at the dissolution front. In the Syracuse Basin of western Kansas and eastern Colorado, Johnson and Timson (2023) identify areas where the lower salt unit is dissolved first and others in which dissolution starts in the upper salt. They infer that the former situation indicates hypogene dissolution whereas the more common latter one reveals epigene dissolution. The dissolution of the Arab and Hith anhydrites in central Saudi Arabia has been ascribed to rising groundwater from the Lower Mega Aquifer System that discharges in the subsidence belt associated with the dissolution front (Kempe and Dirks, 2008; Schleusener et al., 2013). Although the available information of the hydrogeological functioning of this large-scale karst system is rather limited (Al-Hashim et al., 2024), several lines of evidence strongly support the hypogene model: (1) the recharge area for a potential epigene dissolution is very small, while the aquifer units underlying the Arab and Hith formation have vast recharge areas to the west; (2) according to Sharief et al. (1991), in the Ar Riaydh area, boreholes often show that the Arab anhydrite units dissolve before that the overlying Hith anhydrite, suggesting upward advance of the dissolution process; (3) Dahl Hit sinkhole cavern exposes a section around 90 m thick of the Hith Formation, indicating that this karst feature is related to dissolution occurring at the base or close to the base of the Hith Formation (Gregory, 2011). Further hydrogeological investigations, including piezometric and hydrochemical data from specific hydrostratigraphic units are needed to gain deeper insight into this exceptional Ca-sulphate karst system.

According to our literature review, the initiation and progression of dissolution fronts in dipping evaporites can be controlled by a number of extrinsic factors, such as tectonic deformation (e.g., tilting and uplift), base level lowering (e.g., fluvial entrenchment), climate variability impacting on aquifer recharge, and glacial periods with elevated hydraulic heads and enhanced infiltration. The onset of significant interstratal dissolution of the Arab and Hith anhydrites was likely activated by the tilting of the Phanerozoic succession in the Interior Homocline.

This deformation was related to the rifting in the Red Sea, accompanied by the uplift and doming in the Arabian Shield that started around 30–25 Ma (Oligocene; Ghebreab, 1998; Rausch and Dirks, 2024). Gaining deeper insight into this issue would require further investigation on the chronostratigraphy of the sediments filling the dissolution-induced subsidence trough, including the Umm Sha'al formation. Most probably, dissolution and subsidence processes may have operated continuously, but at significantly greater rates during humid periods with greater groundwater recharge over the Cenozoic. According to Rausch and Dirks (2024), during the Holocene "Pluvial Period" groundwater recharge from precipitation was one order of magnitude higher than at the present time.

The available data on the horizontal displacement rate of dissolution fronts in evaporites are scarce and based on loosely constrained ages for the initiation of the process. In central Kansas, Walters (1978) estimated an average rate of 3–6 km Myr^{-1} for the horizontal retreat of the dissolution front in the 90 m thick Permian Hutchinson Salt over the Quaternary. In the Delaware Basin (New Mexico and Texas), Bachman and Johnson (1973) calculated a lateral migration rate of 9 km Myr^{-1} for the dissolutional edge of the Permain Salado Formation after deposition of the Ogalalla Formation (post-4 Myr). No estimates can be given for the dissolution front in the Late Jurassic anhydrites of the Interior Homocline due to the lack of reliable chronological data, but they are expected to be much lower than those reported for salt formations. The equilibrium solubility of halite in pure water at 25 °C, 1 atm and pH 7 is 424 g L^{-1}, while those of anhydrite and gypsum are 3.9 g L^{-1} and 2.6 g L^{-1}, respectively (mass of dissolved solute in 1 L of solution). Halite is characterised by a very rapid transport-controlled dissolution kinetics, while gypsum/anhydrite, display a slower mixed transport- and surface-controlled kinetics (De Waele and Gutiérrez, 2022 and references therein).

Despite evaporite dissolution fronts and the associated structures having received limited attention in the scientific literature, they have multiple practical implications for the development of resources (e.g., salt, oil, gas, coal), geostorage operations (nuclear waste, CO_2, hydrocarbons), hydrochemical degradation of water, and hazard assessments, particularly sinkholes. Sinkhole activity tends to be associated with the dissolution front, the location of which can be inferred on the basis of geomorphic criteria and subsurface data. In the case of central Saudi Arabia and Ar Riyadh city, natural dissolution seems to be very limited at the present time given the low precipitation (ca. 100 mm/yr) and limited aquifer recharge. Nonetheless, recently, a significant number of new collapse sinkholes have occurred in specific areas along the dissolution and subsidence belt. The clear spatial and temporal correlation between those sinkhole sites and anthropogenic activities involving significant water infiltration (artificial lakes, water leakage from pipes, sewage disposal) indicates that these are mostly human-induced sinkholes. An increase in the sinkhole hazard and associated damage are likely to occur in the near future, especially as Ar Riyadh city expands across the dissolution front and adverse human activities become more widespread. A similar situation whereby the sinkhole hazard has significantly increased by anthropogenic hydrological changes has been documented in other regions of Saudi Arabia (Youssef et al., 2016, 2020).

10. Summary and conclusions

The monoclinal folds and subsidence troughs associated with downdip propagating dissolution fronts in gently dipping evaporites (salt and gypsum/anhydrite) are the largest karst features or Earth, reaching as much as 1000 km in length. The documented cases essentially occur in large and slightly deformed (i.e., gentle tilted) evaporite basins that have been the subject of intense geological investigations (North America, Saudi Arabia, United Kingdom). These features likely have gone unnoticed in numerous evaporite basins of the world.

The largest Ca-sulphate karst feature is the dissolution and subsidence belt developed along the updip edge of the Upper Jurassic Hith and Arab anhydrites in the Interior Homocline of central Saudi Arabia, with a minimum length of 800 km, including Ar Riyadh city and occurring in a region with very low precipitation (ca. 100 mm/yr). Moreover, this is the example where the structures and landforms related to dissolution-induced subsidence are best displayed.

The monoclinal folds developed atop the downdip migrating dissolution fronts may display a highly sinuous cartographic trace, with sharp embayments and salients. The bending-moment produces extensional structures in the upper anticlinal hinge (fissures, normal faults, grabens) and buckle folds in synclinal and periclinal hinges. There is a progressive transfer of the rocks from the upper hinge towards the lower hinge as the dissolution front migrates, involving a change in the local stress regime. The structural style of these supra-evaporite drape folds is largely controlled by factors such as the thickness of the evaporite unit, inclination of the dissolution front and the mechanical properties and thickness of the supra-evaporite package. Several criteria are proposed to differentiate between dissolution-induced monoclinal folds and non-gravitational folds that may be underlain by buried seismogenic faults.

The monoclinal fold scarps are often punctured by hectometre-scale caprock collapse sinkholes that may reach high densities and clustering. The large size of the giant caprock collapse sinkholes in central Saudi Arabia, reaching more than 400 m in length, is attributed to both the collapse of large deep-seated cavities and the post-collapse expansion of the sinkholes by mass wasting processes acting on their margins. The caprock collapse sinkholes show an overall chronosequence consistent with the lateral migration of the monocline, with more degraded and mature depressions towards the foot of the scarp.

The subsidence troughs associated with the dissolution fronts may function as laterally migrating depositional basins and may control the surface hydrology, guiding and disrupting drainages and creating lake basins. In most cases, such as in central Saudi Arabia, the limited knowledge on the age of the sediments filling those basins precludes establishing the timing of the main dissolution and subsidence phases and calculating rates for the horizontal migration of the dissolution fronts.

The presence of residual evaporites left behind the dissolution front may be expressed as antiformal highs and peculiar basin and dome morpho-structures. The crater-like enclosed depressions found in the crest of some domes can be attributed to collapse processes acting after passive bending of strata.

The onset of significant interstratal dissolution in the Arab and Hith anhydrites was most probably induced by the eastward tilting of the Interior Homocline, related to rifting in the Red Sea in the Cenozoic. Dissolution is mainly achieved by groundwater from the underlying aquifers (hypogene dissolution) that discharge in the subsidence trough and have an extensive recharge area to the west.

Interstratal evaporite dissolution most probably experienced periods of enhanced activity during humid periods with relatively high aquifer recharge. It is estimated that the average annual precipitation during the "Pluvial Period" (9.5–5 ka) in central Saudi Arabia was around 350–450 mm/yr (Rausch and Dirks, 2024 and references therein). Overall, evaporite dissolution seems to be a very subdued process at the present time, given the aridity of the region (ca. 100 mm/yr). However, sinkholes hazard and risk are experiencing a significant increase in Ar Riyadh area, ascribable to anthropogenic hydrological impacts (e.g., localized water recharge) and the expansion of the city across the dissolution front.

Two important know gaps regarding most of the evaporite dissolution fronts and the associated morpho-structures include the limited understanding of the functioning of the hydrogeological systems responsible for the interstratal karstification, and the scarcity of geochronological data on the timing of this long-term and large-scale dissolution-induced subsidence phenomena.

Declaration of competing interest

Francisco Gutierrez reports financial support was provided by Spanish Government. If there are other authors, they declare that they have no known competing financial interests or personal relationships that could have appeared to influence the work reported in this paper.

Data availability

Data will be made available on request.

Acknowledgements

The work by FG has been supported by the project DIAPERNO (PID2021-123189NB-I00) of the Spanish Government (Ministerio de Ciencia e Innovación). The TanDEM-X digital elevation models were provided by the German Aerospace Center (grant DEM_GEOL4204). FG belongs to the IUCA and the Geoenvironmental Processes and Global Change (E02_23R) research group financed by the Aragón Government and the European Social Fund (ESF-FSE). We are thankful to Dr. Anthony Cooper and two additional reviewers for their insightful comments, as well as to Diego Torromé for providing key references.

References

Al-Hashim, M.H., Al-Aidaros, A., Zaidi, F.K., 2024. Geological and hydrochemical processes driving karst development in southeastern Riyadh. Central Saudi Arabia. Water 16, 1937.
Al-Mojel, A., Razin, P., Dera, G., 2020. High-resolution sedimentology and sequence stratigraphy of the Oxfordian-Kimmeridgian, Hanifa, Jubaila and Arab outcrops along Jabal Tuwaiq, Central Saudi Arabia. J. Afr. Earth Sci. 165, 103803.
Alsharhan, A.S., Kendall, C.G., 1986. Precambrian to Jurassic rocks of Arabian Gulf and adjacent areas: facies, depositional setting and hydrocarbon habitat. AAPG Bull. 70, 977–1002.
Alsharhan, A.S., Kendall, C.G., 1994. Depositional setting of the Upper Jurassic Hith Anhydrite of the Arabian Gulf: an analog to Holocene evaporites of the United Arab Emirates and lake MacLeod of Western Australia. AAPG Bulletin 78, 1075–1096.
Anderson, R.Y., 1981. Deep-seated salt dissolution in the Delaware Basin, Texas and New Mexico. In: Wells, S.G., Lamber, W. (Eds.), Environmental Geology and Hydrogeology in New Mexico New Mexico Geological Society Special Publication, 10, pp. 133–145.
Anderson, N.L., Hinds, R.C., 1997. Glacial loading and unloading: a possible cause of rock salt dissolution in the western Canada basin. Carbonates and Evaporites 12, 43–52.
Anderson, N.L., Knapp, R., 1993. An overview of some of the larger scale mechanisms of salt dissolution in Western Canada. Geophysics 58, 1375–1387.
Anderson, R.Y., Kietze, K.K., Rhodes, D.J., 1978. Development of dissolution breccias, northern Delaware Basin, New Mexico and Texas. In: Geology and Mineral Deposits of Ochoan Rocks in Delaware Basin and Adjacent Areas. New Mexico Bureau of Mines and Mineral Resources, Circular, 159, pp. 47–52.
Anderson, N.L., Hopkins, J., Martinez, A., Knapp, R.W., Macfarlane, P.A., Watney, W.L., Black, R., 1994. Dissolution of bedded rock salt: a seismic profile across the active eastern margin of the Hutchinson Salt Member, Central Kansas. Comput. Geosci. 20, 889–903.
Ayres, M.G., Bilal, M., Jones, R.W., Slentz, L.W., Tartir, M., Wilson, A.O., 1982. Hydrocarbon habitat in main producing areas, Saudi Arabia. AAPG Bulletin 66, 1–9.
Bachman, G.O., 1980. Regional Geology and Cenozoic History of Pecos Region, Southeastern New Mexico. U.S. Geological Survey Open-file Report 80–1099 (116 p).
Bachman, G.O., 1984. Regional geology of Ochoan evaporites, northern part of Delaware Basin. New Mexico Bureau of Mines and Mineral Resources. Circular 184, 22 p.
Bachman, G.O., Johnson, R.B., 1973. Stability of salt in the Permian salt basin of Kansas, Oklahoma, Texas and New Mexico. USGS Open-file report 4339–4, 62 p.
Bamousa, A.O., Daoudi, M., Hachemi, K., 2020. Tectono-geomorphic development of an active transtensional depression: a case study of Mountain Tuwaiq Plateau, south Riyadh City, Saudi Arabia. Carbonates and Evaporites 35 (4), 127.
Birks, S., Moncur, M.C., Gibson, J.J., Yi, Y., Fennell, J.W., Taylor, E.B., 2018. Origin and hydrogeological setting of saline groundwater discharges to the Athabasca River: Geochemical and isotopic characterization of the hyporheic zone. Appl. Geochem. 98, 172–190.
Blakey, R.C., 1990. Stratigraphy and geologic history of Pennsylvanian and Permian rocks, Mogollon Rim region, Central Arizona and vicinity. Geol. Soc. Am. Bull. 102, 1189–1217.
Breton, J.P., Brosse, J.M., Cavelier, C., Fourniguet, J., Le Nindre, M., Manivit, J., Vaslet, D., Vincent, P.L., 1984. Evolution structural des grabens du centre l'Arabia du Crétacé au Quaternaire. Ann. Soc. Geol. Nord 103, 297–307.
Broughton, P.L., 1977. Origin of coal basins by salt solution. Nature 270, 420–423.
Broughton, P.L., 2013. Devonian salt dissolution-collapse breccias flooring the cretaceous Athabasca oil sands deposit and development of lower McMurray Formation sinkholes, northern Alberta Basin, Western Canada. Sediment. Geol. 283, 57–82.
Broughton, P.L., 2015. Syndepositional architecture of the northern Athabasca oil sands deposit, northeastern Alberta. Can. J. Earth Sci. 52, 21–50.
Broughton, P.L., 2017. Hypogene karst collapse of the Devonian Prairie Evaporite basin in western Canada. In: Klimchouk, A., Palmer, A.N., De Waele, J. (Eds.), Hypogene Karst Regions and Caves of the World. Cave and Karst Systems of the World. Springer, Dordrecht, pp. 617–632.
Broughton, P.L., 2018a. Ghost-rock karstification of Devonian limestone flooring the Athabasca Oil Sands in western Canada. Geomorphology 318, 303–319.
Broughton, P.L., 2018b. Orogeny and the collapse of the Devonian Prairie Evaporite karst in Western Canada: impact on the overlying cretaceous Athabasca Oil Sands. Geol. Soc. Lond. Spec. Publ. 466, 25–78.
Broughton, P.L., 2021. Alignment of saline springs with evaporite karst structures in Northeast Alberta, western Canada: analogue for cretaceous hypogene brine seeps to the surface. Acta Carsologica 50, 119–141.
Conway, B., Cook, J., 2013. Monitoring evaporite karst activity and land subsidence in the Holbrook Basin, Arizona using Interferometric Synthetic Aperture Radar (InSAR). In: Land, L., Doctor, D.H., Stephenson, J.B. (Eds.), Sinkholes and the Engineering and Environmental Impacts of Karst. National Cave and Karst Research Institute, Carlsbad, 187–194 p.
Cooper, A.H., 1998. Subsidence hazards caused by the dissolution of Permian gypsum in England: Geology, investigation and remediation. In: Maund, J.G., Eddleston, M. (Eds.), Geohazards in Engineering Geology, Geological Society, London, Engineering Geology Special Publications, vol. 15, pp. 265–275.
Cooper, A.H., 2002. Halite karst geohazards (natural and man-made) in the United Kingdom. Environ. Geol. 42, 505–512.
Cooper, A.H., 2020. Geohazards caused by gypsum and anhydrite in the UK: Including dissolution, subsidence, sinkholes and heave. In: Giles, D.P., Griffiths, J.S. (Eds.), Geological Hazards in the UK: Their Occurrence, Monitoring and Mitigation, Geological Society, London, Engineering Geology Special Publications, vol. 29, pp. 403–423.
Cueto, M., Olona, J., Fernández-Viejo, G., Pando, L., López-Fernández, C., 2018. Karst-induced sinkhole detection using an integrated geophysical survey: a case study along the Riyadh Metro Line 3 (Saudi Arabia). Near Surface Geophysics 16, 270–281.
De Mille, G., Shouldice, J.R., Nelson, H.W., 1964. Collapse structures related to evaporites of the Prairie Formation. Saskatchewan. Geological Society of America Bulletin 75, 307–316.
De Waele, J., Gutiérrez, F., 2022. Karst Hydrogeology. Wiley, Geomorphology and Caves, 888 p.
Dini, S., Wallace, C.A., Halawani, M.A., Al-Sobhi, S.A., Kashghari, W.A., Al-Ghamdi, A.S., 2009. Explanatory notes to the geologic map of the as Sulayyil Quadrangle, Kingdom of Saudi Arabia. In: Geoscience Map GM-141C, Scale 1:250,000, Sheet 20H. Saudi Geological Survey, 64 p.
Epstein, J.B., 2003. Gypsum karst in the Black Hills, South Dakota-Wyoming: Geomorphic Development, Hazards, and Hydrology. In: Johnson, K.S., Neal, J.T. (Eds.), Evaporite Karst and Engineering/Environmental Problems in the United States, Norman: Oklahoma Geological Survey Circular, vol. 109, pp. 241–254.
Frye, J.C., 1950. Origin of Kansas Great Plains depressions. Kansas Geological Survey Bulletin 86, 1–20.
Fuest, T., Al-Shabibi, I., Dirks, H., Rausch, R., 2012. Hydrogeology of the late Permian, Triassic and Jurassic aquifers of Saudi Arabia. In: Rausch, R., Schütt, Ch., Himmelsbach, T. (Eds.), Hydrogeology of Arid Environments. Bomtraeger Science Publisher, p. 128.
Ghebreab, W., 1998. Tectonics of the Red Sea region reassessed. Earth Sci. Rev. 45, 1–44.
Gökkaya, E., Gutiérrez, F., Ferk, M., Görüm, T., 2021. Sinkhole development in the Sivas gypsum karst, Turkey. Geomorphology 386, 107746.
Gregory, G., 2011. The Desert Cave Project. http://www.saudicaves.com/ainhit2/index.html. Last accessed on September 2024.
Gutiérrez, F., Cooper, A.H., 2013. Surface morphology of gypsum karst. In: Frumkin, A. (Ed.), Treatise of Geomorphology. Karst Geomorphology, 6. Elsevier, Amsterdam, pp. 425–437.
Gutiérrez, F., Lizaga, I., 2016. Sinkholes, collapse structures and large landslides in an active salt dome submerged by a reservoir: the unique case of the Ambal ridge in the Karun River, Zagros Mountains. Iran. Geomorphology 254, 88–103.
Gutiérrez, F., Carbonel, D., Kirkham, R.M., Guerrero, J., Lucha, P., Matthews, V., 2014. Can flexural-slip faults related to evaporite dissolution generate hazardous earthquakes? The case of the Grand Hogback monocline of west-Central Colorado. Geol. Soc. Am. Bull. 126, 1481–1494.
Gutiérrez, F., Fabregat, I., Roqué, C., Carbonel, D., Zarroca, M., Linares, R., Yechieli, Y., García-Arnay, A., Sevil, J., 2019. Sinkholes in hypogene versus epigene karst systems, illustrated with the hypogene gypsum karst of the Sant Miquel de Campmajor Valley, NE Spain. Geomorphology 328, 57–78.
Hancock, P.L., Al-Kadhi, A., 1978. Analysis of mesoscopic fractures in the Dhruma-Nisah segment of the central Arabian graben system. Journal of Geological Society, London 135, 339–347.
Hill, C.A., 1996. Geology of the Delaware Basin, Guadalupe, Apache, and Glass Mountains, New Mexico and West Texas. Permian Basin Section-SEPM. Publication No. 96–39.
Hill, C.A., 2003. Interstratal karst at the waste isolation pilot plant site, southeastern New Mexico. In: Johnson, K.S., Neal, J.T. (Eds.), Evaporite Karst and Engineering/Environmental Problems in the United States, Norman: Oklahoma Geological Survey Circular, vol. 109, pp. 197–210.

Hopkins, J.C., 1987. Contemporaneous subsidence and fluvial channel sedimentation: Upper Mannville C Pool, Berry Field, lower cretaceous of Alberta. AAPG Bulletin 71, 334–345.
Johnson, K.S., 1989. Development of the Wink Sink in Texas, USA, due to salt dissolution and collapse. Environ. Geol. Water Sci. 14, 81–92.
Johnson, K.S., 2021a. Overview of evaporite karst in the Greater Permian Evaporite Basin (GPEB) of Texas, New Mexico, Oklahoma, Kansas, and Colorado, USA. In: Johnson, K.S., Land, L., Decker, D.D. (Eds.), Evaporite Karst in the Greater Permian Evaporite Basin (GPEB) of Texas, New Mexico, Oklahoma, Kansas, and Colorado, Oklahoma Geological Survey, Circular, vol. 113, pp. 1–37.
Johnson, K.S., 2021b. Dissolution of the Permian Flowerpot Salt beneath the Great Plains Resoervoirs, Queens State Wildlife area, in Kiowa, Prowers, and Bent Counties, Southeast Colorado. In: Johnson, K.S., Land, L., Decker, D.D. (Eds.), Evaporite Karst in the Greater Permian Evaporite Basin (GPEB) of Texas, New Mexico, Oklahoma, Kansas, and Colorado, Oklahoma Geological Survey, Circular, vol. 113, pp. 337–346.
Johnson, K.S., 2021c. Salt dissolution and the Wallace sinkholes in the Sharon Springs-Wallace area, Wallace County, Western Canada. In: Johnson, K.S., Land, L., Decker, D.D. (Eds.), Evaporite Karst in the Greater Permian Evaporite Basin (GPEB) of Texas, New Mexico, Oklahoma, Kansas, and Colorado, Oklahoma Geological Survey, Circular, vol. 113, pp. 319–335.
Johnson, K.S., Timson, G.H., 2023. Salt dissolution in the Permian Flowerpot and Blaine formations defines limits of the Syracuse Basin in western Kansas and eastern Colorado. Midcontinent Geoscience 4, 1–41.
Kalbus, E., Oswald, S., Wang, W., Kolditz, O., Engelhardt, I., Al-Saud, M.I., Rausch, R., 2011. Large-scale modeling of the groundwater resources on the Arabian platform. International Journal of Water Resources and Arid Environments 1, 38–47.
Karpoff, R., 1956. Sur quelques failles et grabens de l'Arabie centrale et septentrionale. In: Comptes Rendus Sommaires de la Société Géologique de France, pp. 294–296.
Kempe, S., Dirks, H., 2008. Layla Lakes, Saudi Arabia: the world-wide largest lacustrine gypsum tufas. Acta Carsologica 37, 7–14.
Kirkham, R.M., Streufert, R.K., Kunk, M.J., Budahn, J.R., Hudson, M.R., Perry Jr., W.J., 2002. Evaporite tectonism in the lower Roaring Fork river valley, westcentral Colorado. In: Kirkham, R.B., Scott, R.B., Judkins, T.W. (Eds.), Late Cenozoic Evaporite Tectonism and Volcanism in West-Central Colorado. 73-99, 366. Geological Society of America Special Paper, pp. 73–99.
Land, L., 2003. Evaporite karst and regional groundwater circulation in the lower Pecos Valley of Southeastern New Mexico. In: Johnson, K.S., Neal, J.T. (Eds.), Evaporite Karst and Engineering/Environmental Problems in the United States, Oklahoma Geological Survey Circular, vol. 109, pp. 227–232.
Land, L., 2016. Field trip: Evaporite karst of the lower Pecos Valley, New Mexico. New Mexico Bureau of Geology and Mineral Resources. National Cave and Karst Research Institute. KIP Articles 5838.
Lindsay, R.F., Cantrell, D.L., Hughes, G.W., Keith, T.H., Mueller III, H.W., Russell, S.D., 2006. Ghawar Arab-D reservoir: widespread porosity in shoaling-upward carbonate cycles, Saudi Arabia. In: Harris, P.M., Weber, L.J. (Eds.), Giant hydrocarbon reservoirs in the world: From rocks to reservoir characterization and modelling. AAPG Memoir 88, SEPM Special Publication, pp. 97–137.
McCalpin, J.P., 2005. Late Quaternary activity of the Pajarito fault, Rio Grande rift of northern New Mexico, USA. Tectonophysics 408, 213–236.
Memesh, A., Dini, S., Gutiérrez, F., Wallace, C.A., 2008. Evidence of large-scale subsidence caused by interstratal karstification of evaporites in the Interior Homocline of Central Saudi Arabia. European Geosciences Union General Assembly. Geophys. Res. Abstr. 10, A–02276.
Memesh, A.M., Dini, S.M., Al-Amoudi, S.A., Wallace, C.A., Sobhi, S.A., Al-Juaid, A.J., 2010. Explanatory notes to the geologic map of the Hawtat Bani Tamim Quadrangle, Kingdom of Saudi Arabia. In: Geoscience Map GM-143C, Scale 1:250,000, Sheet 23I. Saudi Geological Survey, 63 p.
Memesh, A.M., Dini, S.M., Bamousa, A.O., Al-Amoudi, S.A., Al-Juaid, A.J., 2011. Explanatory notes to the geologic map of the Rumah Quadrangle, Kingdom of Saudi Arabia. In: Geoscience Map GM-145C, Scale 1:250,000, Sheet 25I. Saudi Geological Survey, 45 p.
Memesh, A.M., Dini, S.M., Bamousa, A.O., Al-Tassan, A., Al-Zahrani, A.M., Nabhan, A.I., 2012. Explanatory notes to the geologic map of the Al Artawiyah Quadrangle, Kingdom of Saudi Arabia. In: Geoscience Map GM-146C, Scale 1:250,000, Sheet 26H. Saudi Geological Survey, 42 p.
Michelsen, N., Dirks, H., Schulz, S., Kempe, S., Al-Saud, M., Schüth, C., 2016. YouTube as a crowd-generated water level archive. Sci. Total Environ. 568, 189–195.
Murris, R.J., 1980. Middle East: stratigraphic evolution and oil habitat. AAPG Bulletin 64, 597–618.
Neal, J.T., 1995. Supai salt karst features: Holbrook Basin, Arizona. In: Beck, B.F. (Ed.), Karst Geohazards. Engineering and Environmental Problems in Karst Terrane. Balkema, Rotterdam, pp. 53–59.
Neal, J.T., 1998. Evaporite karst in the Holbrook Basin, Arizona. In: Borchers, J.W. (Ed.), Land Subsidence Case Studies and Current Research, Association of Engineering Geologists. Special Publication, vol. 8, pp. 383–384.
Neal, J.T., Colpitts, R.M., 1997. Richard Lake, an evaporite karst depression in the Holbrook Basin, Arizona. Carbonates Evaporites 12, 91–98.
Neal, J.T., Johnson, K.S., 2003. A compound breccia pipe in evaporite karst: McCauley sinks, Arizona. In: Johnson, K.S., Neal, J.T. (Eds.), Evaporite Karst and Engineering/Environmental Problems in the United States, Norman: Oklahoma Geological Survey Circular, vol. 109, pp. 305–314.
Neal, J.T., Johnson, K.S., Lindberg, P., 2013. Variations in evaporite karst in the Holbrook Basin, Arizona. In: Land, L., Doctor, D.H., Stephenson, J.B. (Eds.), Sinkholes and the Engineering and Environmental Impacts of Karst. Carlsbad, National Cave and Karst Research Institute, pp. 177–186.
Oldham, D.W., 1996. Permian salt in the northern Denver basin: Controls on occurrence and relationship to oil and gas production from cretaceous reservoirs. In: Longman, M.W., Sonnenfeld, M.D. (Eds.), Paleozoic Systems of the Rocky Mountain Region: Rocky Mountain Section of the Society of Economic Paleontologists and Mineralogists, Denver, Colorado, pp. 335–354.
Olive, W.W., 1957. Solution-subsidence troughs, Castile Formation of Gypsum Plain, Texas and New Mexico. Geol. Soc. Am. Bull. 68, 351–358.
Parker, J.M., 1967. Salt solution and subsidence structures, Wyoming, North Dakota and Montana. AAPG Bulletin 51, 1929–1947.
Parkhurst, D.L., Appelo, C.A.J., 2013. Description of Input and examples for PHREEQC Version 3. A Computer Program for Speciation, batch Reaction, one Dimensional Transport, and Inverse Geochemical Calculations. In: Techniques and Methods, Book 6, Chap. A43. Denver, Colorado: U.S. Geological Survey.
Pollastro, R.M., Karshbaum, A.S., Viger, R.J., 1988. Maps showing geology, oil and gas fields and geologic provinces of the Arabian Peninsula. USGS Open-File Report 97–470B.
Powell, J.W., 1873. Geological structure of a district of country lying to the north of the Grand Canyon of the Colorado. Am. J. Sci. 5, 456–465.
Powers, R.W., 1968. Saudi Arabia. In: Lexique Stratigraphique International. Centre National de la Recherche Scientifique, Paris, V. III.
Powers, R.W., Ramirez, L.F., Redmon, C.D., Elberg, E.I., 1966. Geology of the Arabian Peninsula: Sedimentary geology of Saudi Arabia. Professional Paper 560D.
Quinlan, J.F., Smith, R.A., Johnson, K.S., 1986. Gypsum karst and salt karst of the United States of America. Le Grotte d'Italia 13, 73–92.
Rahn, P.H., Davis, A.D., 1996. Gypsum foundation problems in the Black Hills area, South Dakota. Environ. Eng. Geosci. 2, 213–223.
Rausch, R., Dirks, H., 2024. A hydrogeological overview of the Upper mega Aquifer System on the Arabian Platform. Hydrgeol. J. 32, 621–634.
Rausch, R., Simon, T., Al Ajmi, H., Dirks, H., 2014a. The scarp lands of Saudi Arabia. Arabian Journal of Geosciences 7, 2437–2450.
Rausch, R., Simon, T., Al Ajmi, H., Dirks, H., 2014b. The scarp lands of Saudi Arabia. Arab. J. Geosci. 7, 2437–2450.
Schleusener, F., Kempe, S., Dirks, H., Rausch, R., Göbel, P., 2013. Die erdfälle von Layla und Al-Kharj – einblicke in die karst-hydrogeologie des oberen Jura von Saudi-Arabien. Grundwasser 18, 271–276.
Sevil, J., Gutiérrez, F., 2023. Morphometry and evolution of sinkholes on the western shore of the Dead Sea. Implications for susceptibility assessment. Geomorphology 434, 108732.
SGS, 2021. Stratigraphy of the Phanerozoic Cover Rocks of Saudi Arabia, Saudi Geological Survey Special Publication SGS-sp-2021-2, One Colored Chart.
Sharief, F.A., Khan, M.S., Magara, K., 1991. Outcrop-Subcrop Sequence and Diagenesis of Upper Jurassic Arab-Hith Formations, Central Saudi Arabia. J. KAU Earth Science 4, 105–136.
Stafford, K.W., Land, L., Klimchouk, A.B., 2008. Hypogenic speleogenesis within seven Rivers evaporites: Coffee Cave, Eddy County, New Mexico. Journal of Cave and Karst Studies 70, 47–61.
Steineke, M., Bramkamp, R.A., Sander, N.J., 1958a. Stratigraphic relations of Arabian Jurassic oil. In: Habitat of Oil. American of Petroleum Geologists Symposium, Tulsa, pp. 1294–1329.
Steineke, M., Bramkamp, R.A., Sander, N.J., 1958b. Stratigraphic relations of Arabia Jurassic habitat of oil. American Association of Petroleum Geology Bulletin 37, 1252–1278.
Stoakes, F., Verhoef, M., Mahood, R., 2014. Multiphase solution removal of the Prairie Evaporite Formation in northeast Alberta. In: Canadian Society of Petroleum Geologists, 2014 Annual Meeting, Calgary, Alberta, Extended Abstract.
Supajanya, T., Friederich, M.C.Ç., 1992. Salt tectonics of the Sakon Nakhon Basin, Northeast Thailand. Journal of the Southeast Asian Earth Sciences 7, 258–259.
Utha-aroon, C.L., Coshell, L., Warren, J.K., 1995. Early and late dissolution in the Maha Sarakham Formation: Implications for basin stratigraphy. In: International Conference on Geology. Geochronology and Mineral Resources of Indochina, Khon Kaen, Thailand, pp. 275–286.
Vaslet, D., Brosse, J.M., Breton, J.P., Manivit, J., Le Strat, P., Fourniguet, J., Shorbaji, H., 1988. Explanatory Notes to the Geologic Map of the Shaqra Quadrangle, Kingdom of Saudi Arabia. Geoscience Map GM-12oC, Scale 1:250,000, Sheet 25H. Ministry of Petroleum and Mineral Resources, Kingdom of Saudi Arabia, p. 29.
Vaslet, D., Al-Muallem, M.S., Maddah, S.S., Brosse, J.M., Fourniguet, J., Breton, J.P., Le Nindre, Y.M., 1991. Explanatory Notes to the Geologic Map of the Ar Riyad Quadrangle, Kingdom of Saudi Arabia. Geoscience Map GM-121, Scale 1:250,000, Sheet 24I. Deputy Ministry for Mineral Resources, Kingdom of Saudi Arabia, p. 54.
Walker, J., Almási, I., Stoakes, F., Potma, K., O'Keefe, J., 2017. Hypogenic karst beneath the Athabasca Oil Sands: Implications for oil sands mining operations. Bull. Can. Petrol. Geol. 65, 115–146.
Walters, R.F., 1978. Land Subsidence in Central Kansas Related to Salt Dissolution. Bulletin of Kansas University Geological Survey 214, 1–82.
Waltham, T., 2005. Tiankengs of the world, outside China. Cave and Karst Science 32, 1–12.
Warren, J.K., 2016. Evaporites: A Geological Compendium. Springer-Verlag, Heidelberg, 1813 p.
Weijermars, R., 1998. Plio-Quaternary movement of the East Arabian block. GeoArabia 3, 509–540.
Wessel, B., 2016. TanDEM-X Ground Segment – DEM Products Specification Document. EOC, DLR, Oberpfaffenhofen, Germany, Public Document TD-GS-PS-0021, Issue 3.2, 2016. Available: https://tandemx-science.dlr.de/.
Wilson, A.O., 2020. The Middle to late Jurassic Arabian Intrashelf Basin of the Eastern Arabian Peninsula. Geological Society Memoir 53, 213 p.

Wolpert, P., Bartenbach, M., Suess, P., Rausch, R., Aigner, T., Le Nindre, Y.M., 2015. Facies analysis and sequence stratigraphy of the uppermost Jurassic–Lower Cretaceous Sulaiy Formation in outcrops of central Saudi Arabia. GeoArabia 20, 67–122.

Wolpert, P.J., Bartenbach, M., Aigner, T., Wilson, A.O., Al-Husseini, M.I., Petrovic, A., Dirks, H., Rausch, R., 2024. Sedimentological and sequence-stratigraphic analyses of the Tithonian Hith Anhydrite Formation in the Dahal Hit outcrop. Saudi Arabia. Arabian Journal of Geosciences 17, 135.

Youssef, A.M., Al-Harbi, H.M., Gutiérrez, F., Zabramwi, Y.A., Bulkhi, A.B., Zahrani, S.A., Bahamil, A.M., Zaharani, A.J., Otaibi, Z.A., El-Haddad, B.A., 2016. Natural and human-induced sinkhole hazards in Saudi Arabia: distribution, investigation, causes and impacts. Hydrgeol. J. 24, 625–644.

Youssef, A.M., Zabramwi, Y.A., Gutiérrez, F., Bahamil, A.M., Otaibi, Z.A., Zahrani, A.J., 2020. Geophysical investigation (ERT) of a sinkhole induced by uncontrolled groundwater withdrawal, Al Jouf Region, Saudi Arabia. J. Arid Environ. 177, 104132.